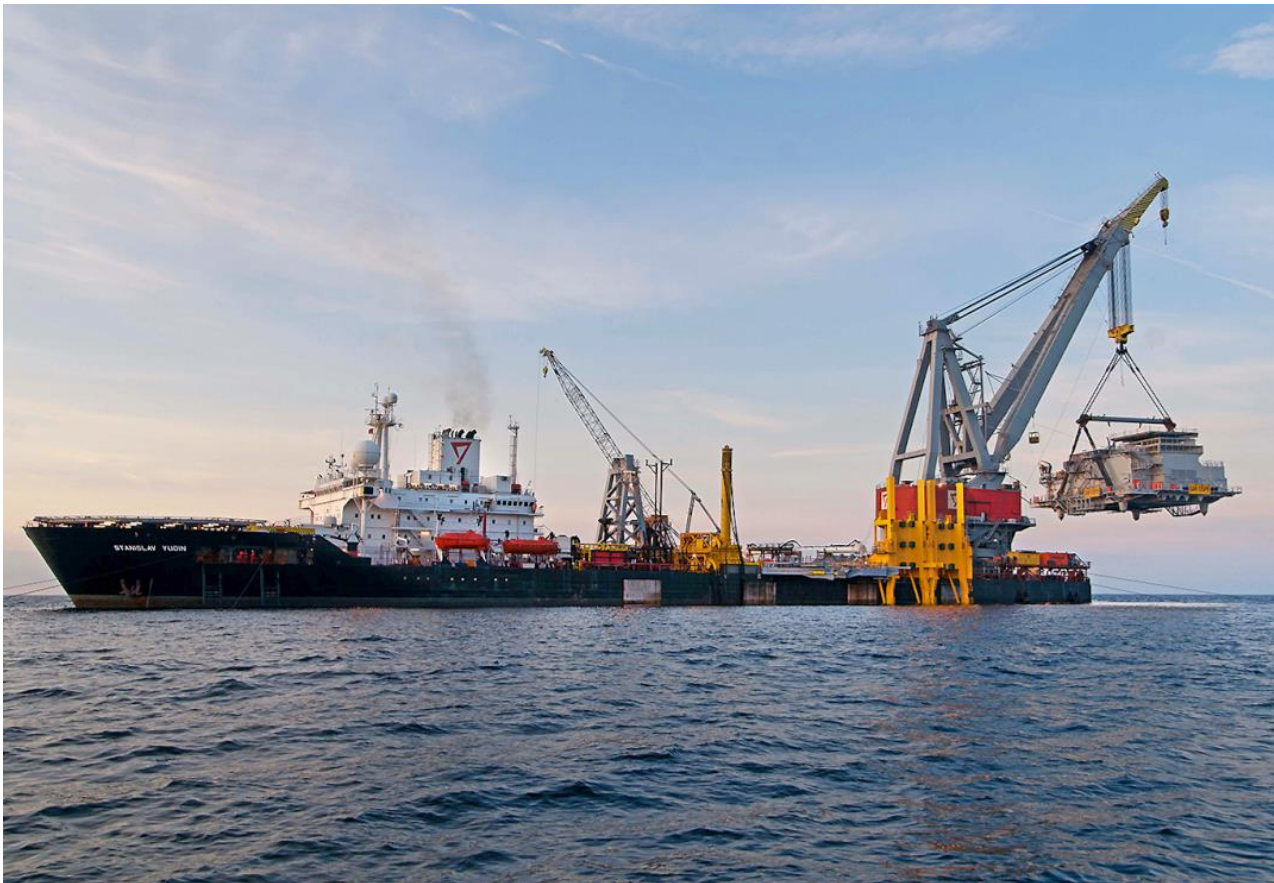




CHALMERS



Finite Element Analysis of a Lifting Portable Offshore Unit

A comparison between a shell and a beam model

Master's thesis in Applied Mechanics

CHRISTIAN LIEBERT

MAHAM RASHID

MASTER'S THESIS IN APPLIED MECHANICS

Finite Element Analysis of a Lifting Portable Offshore Unit

A comparison between a shell and a beam model

CHRISTIAN LIEBERT
MAHAM RASHID

Department of Applied Mechanics
Division of Material and Computational Mechanics
CHALMERS UNIVERSITY OF TECHNOLOGY

Göteborg, Sweden 2015

Finite Element Analysis of a Lifting Portable Offshore Unit
A comparison between a shell and a beam model
CHRISTIAN LIEBERT
MAHAM RASHID

© CHRISTIAN LIEBERT, MAHAM RASHID, 2015

Master's thesis 2015:09
ISSN 1652-8557
Department of Applied Mechanics
Division of Material and Computational Mechanics
Chalmers University of Technology
SE-412 96 Göteborg
Sweden
Telephone: +46 (0)31-772 1000

Cover:
Seaway Heavy Lifting Orders OCTOPUS-Onboard (2014). [Accessed 27 May 2015]

Chalmers Reproservice
Göteborg, Sweden 2015

Finite Element Analysis of a Lifting Portable Offshore Unit
A comparison between a shell and a beam model
Master's thesis in Applied Mechanics
CHRISTIAN LIEBERT
MAHAM RASHID
Department of Applied Mechanics
Division of Material and Computational Mechanics
Chalmers University of Technology

ABSTRACT

The offshore industries have a big demand of transferring heavy objects in portable offshore (PO) units between oil rigs and boats and this is done by lifting. The offshore company Aker Solutions is interested of determining if the same capacity results can be obtained by using a beam model instead of a shell model. The main objective of the present project was to determine if it was possible to model the portable offshore unit with a beam model instead of a shell model. The shell model is the method used presently and is time consuming. If the possibility exists to use a beam model instead of a shell model, a lot of time could be saved during the model setup phase and in the simulation phase which would be of a great importance for the offshore industries. Model modifications were also checked to examine its influence to the results.

The tools used to examine the capacities of these two models have been the FE software Abaqus CAE 6.13-1 and the calculation software MATLAB. The focus in this research was to create and simulate the shell and the beam models in order to compare them. The shell model used thin conventional linear shell elements with Kirchhoff's plate theory which simulated large deformation and was implemented with a multi-linear elastic-plastic material with nonlinear deformation, in order to properly represent the ultimate bearing capacity. The beam model used linear beam elements with Timoshenko beam theory with the same nonlinear material behavior as in the shell model.

The beam model had a higher capacity than the shell model as expected since beam structures are known to be more stiff in general. It is not possible to use a beam model in order to obtain the same capacity result. Internal modification such as the integration points through the thickness were examined for the shell model and it showed that five integration points are the minimum requirement to obtain a converged result for this load case. The contribution of the riser mass (payload) on each support individually is more conservative than applying the mass uniformly on the supports from one master point. The beam model converges at larger element sizes than the shell model. The shell model experience collapse earlier than the beam model, which means that the shell model is more conservative when measuring collapse load. One reason for this is how the mass is applied to the basket in the models. Another reason is the beam element can not deform in its cross section, which makes it stiffer than the shell element. These results are based on one simple load case and a analysis of a couple of more load cases would be preferred for future work in order to make a more general conclusions about collapse load and if it would be possible to use beam elements instead of shell elements when modeling the PO unit.

Keywords: Offshore, PO unit, Basket, FEM, Capacity, Collapse, Shell, Beam, Risers

PREFACE

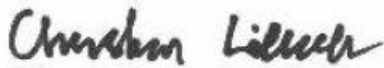
This master's thesis project has been carried out at the consultant company Alten for the offshore company Aker Solutions in Oslo. This research was accomplished at the Division of Material and Computational Mechanics as a last course in the master's program Applied Mechanics at Chalmers University of Technology, Gothenburg. The work has been performed in a time period of 20 weeks, between January and June of 2015.

ACKNOWLEDGEMENTS

We take this opportunity to express our sincere gratitude to our academic supervisor and examiner Professor Ragnar Larsson for his big effort and advice throughout the project. We would also like to thank our supervisor Mikael Almquist at the consultant company Alten for his sincere help and consultation during the past few months. Last but not least we would want to express our gratitude to our supervisor Tobias Tivert at the offshore company Aker Solutions for giving us useful advise and hints to proceed with the project.

We also appreciate our co-workers Sami, Mohsen, Simon and Robin for keeping us in a positive environment at work. It has been a pleasure to proceed this research at Alten.

Göteborg, June 2015



Christian Liebert



Maham Rashid

NOMENCLATURE

PO = Portable Offshore
COM = Center of Mass
MGW = Mass Gross Weight
ML = Master Link
DF = Design Factor
DOF = Degrees of Freedom
BCs = Boundary Conditions
FE = Finite Element

CONTENTS

Abstract	i
Preface	iii
Acknowledgements	iii
Nomenclature	v
Contents	vii
1 Introduction	1
1.1 Problem Description	1
1.2 Deliverable and Limitations	1
1.3 Methodology	2
2 Theory	3
2.1 Element Types	3
2.2 Shell Structures	4
2.2.1 Shell Element Geometry	4
2.2.2 Shell Thickness and Integration Points	4
2.2.3 Thick and Thin Shells	5
2.3 Beam Structures	6
2.3.1 Timoshenko Beam Theory	6
2.4 Material Model	7
2.4.1 Elastic-plastic Material Model	8
2.4.2 Hardening Plastic Behavior	9
2.5 Newton's Method	10
3 Finite Element Representation of PO unit	11
3.1 Geometry	11
3.2 Material Properties	13
3.3 Acceptance Criteria	13
4 FE Analysis of Normal Lift	15
4.1 Methodology in Abaqus CAE	15
4.1.1 Model Simplifications	15
4.1.2 Model Setup	16
4.1.3 Constraints	20
4.1.4 Boundary Conditions and Load	21
4.1.5 Mesh	22
4.2 Convergence Analysis	23
4.3 Placement of the Local Coordinate System	23
4.4 Critical Area	24
5 Results and Discussion	25
5.1 Mesh Convergence	25
5.2 Distribution of Payload due to the Risers	26
5.3 Capacity Analysis - Collapse Load	27
5.4 First and Second Order Elements	28
5.5 Thickness Integration Points	28
5.6 Comparison between the Shell and the Beam model	29
6 Conclusions	31

7 Future Work	32
References	33
Appendix A Kirchhoff's Plate Theory	34
Appendix B Finite Element Equations	36
B.1 Quadrilateral Element	36
B.2 Triangular Element	38
B.3 Beam Element	39
Appendix C Material Properties	42
Appendix D Go Beam	43
D.1 Input data for the shell model	43
D.2 Input data for the beam model	43
Appendix E Mesh Convergence	44
Appendix F Effect of Nonstructural Mass	45

1 Introduction

Usually in the offshore industry the equipments and the products need to be shipped from one place to another. Regularly upon arrival it must be lifted off the ship with cranes. The equipment in the offshore industry can be for instance risers as in this case or other heavy equipment. The structures lifting these heavy objects are called Portable Offshore (PO) units. The specific PO unit in this thesis has the form of a basket. The basket consists of several parts, such as hollow beams, screw nuts and padeyes, which together gives the assembled PO unit. It is important that the lifts are done in a safe and secure way so that no damages take place during or after the lifting processes. To achieve this the Norwegian standard *Det Norske Veritas* (DNV) [1] is used by Aker Solutions, and many other offshore companies. The standard works as a guidance and it includes i.e acceptance criterion and working procedures. It is crucial to do the tests in beforehand with finite element method (FEM). Since the lifting processes are very common in the offshore industry, there exist researches to assure the safety of the basket during lifting. [5][14]. In this project the software Abaqus 6.13-1 has been used, which is a pre-processor solver and a post-processor for finite element analysis. The interesting result from a normal lift case is the capacity of the PO unit with respect to deformation. This research is mainly initiated to compare the differences between a shell and a beam model, when analysing the normal lift case. The reason for comparing these two models is the curiosity and interest of finding similarities in result for these two models. If there is a possibility to achieve the same result with a model made of beam elements as a shell model with shell elements, it is of a great interest to use it in further analyses since it reduces the working hours tremendously. This master's thesis is a pre-study for the offshore company Aker Solutions. Lifting is the most common type of calculation in the offshore industry. In the end of a delivery process, most of the equipment need to be shipped and lifted onto a rig. These lifts must be done in a safe way for the structures so that no cracks or damages occur. The calculations are in many cases straightforward but very time consuming due to computation of heavy elements. In worst case one need to use solid elements, but in most of the cases shell elements are enough. It takes a lot of time to build up a shell model from a solid model compared to building up a beam model. The concept of building up the shell model from a solid CAD model is also known as "cleaning the model". It would have been beneficial if it would have been possible to model the PO unit as a beam model instead of a shell model. A model made of beam elements is much more efficient due to time limitations when building it and running the simulation. If the same results are obtained in less time, a lot of money can be saved.

1.1 Problem Description

The research is initiated due to lack of time to investigate if it is possible to obtain equivalent result between a model meshed with shell elements and a model meshed with beam elements. In the current state, the analyses are made on shell structures which is time consuming to clean from a CAD model. It is of interest to know if a beam structure can be implemented instead of a shell structure in the analyses, and to know which properties are changed due to the element change. The interest lays in how to make the results be as similar as possible with the two models made of shell and beam.

1.2 Deliverable and Limitations

The scope of this master's thesis is to evaluate the capacity of a PO unit lifting a heavy payload and examine the difference in results when this is modeled with shell or beam elements. The result that will be examined is the displacement at a critical location when the gravity load is increased gradually. Mesh convergence analysis will be performed in order to find its influence and requirements on the accuracy of the results. Two different techniques of applying the payload (riser mass) will be analysed for both the model made of shells and beams. Collapse load will be compared for the two payload cases. The influence of the number of the integration points through the thickness will be analysed for the shell structure. Linear and quadratic elements will be compared for both the shell and the beam model. The project scope has been determined in discussion with the supervisor at the university and at Alten. The project limitations set for the thesis are:

- Finite element analysis will be made on one PO unit. The 3D CAD model will be received from the offshore company Aker Solutions in order to save time of constructing a model.
- Only one load case will be analyzed: Normal lift. This case will be analysed in depth.

- The capacity analyses will be following the offshore standard DNV 2.7-3 [1].
- The model will be simplified in order to make the computation easier. Secondary parts will be deleted from the model since they do not affect the stiffness of the structure when the load is applied to the model.

1.3 Methodology

The project will start off with simplifying and cleaning the shell model and also building up the beam model in the CAE software Abaqus 6.13-1. The shell model will use thin conventional linear shell elements rather than continuum shell elements in order to save simulation time. Kirchhoff's plate theory will be used to simulate large deformation and the material model will use multi-linear elastic-plastic properties with non-linear deformation, in order to properly represent the ultimate bearing capacity. The beam model will use linear beam elements with Timoshenko beam theory with the same non-linear material behavior as the shell model. Loads and boundary conditions (BCs) will be added into the model. Different ways of applying the riser load will be analysed and discussed. When the simulations have been completed the results will be interpreted and analyzed using the calculation program MATLAB.

2 Theory

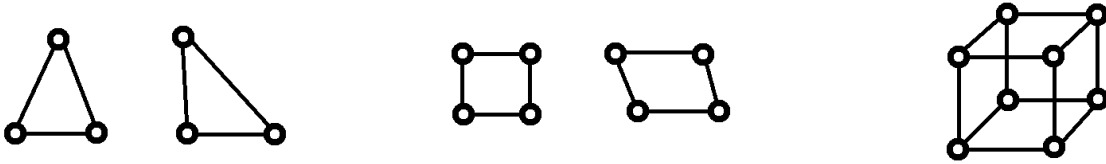
The finite element method (FEM) is a numerical technique for finding approximate solutions to differential equations controlled by boundary values, such as Neumann and Dirichlet BCs. The element stiffness matrix \mathbf{K}_e will in this chapter be derived for linear Triangular and quadrilateral shell elements and for linear beam elements, which later can be used to assemble the global stiffness matrix \mathbf{K} . This is derived so the reader can have a brief understanding of how the software Abaqus is working. In order to calculate the displacement for each node, Eq. (2.1) is used

$$\mathbf{a} = \mathbf{K}^{-1} \mathbf{f} \quad (2.1)$$

where \mathbf{a} contains the displacements and rotations, and \mathbf{f} contains the forces and moments for each of the nodes.

2.1 Element Types

In this project, the basket will be meshed with linear elements and therefore the theory behind constructing the \mathbf{K}_e matrix for the different type of elements will be derived. The elements in the shell model are the conventional linear shell elements and are the most basic ones for a shell model in Abaqus. There are two different types of shell elements used in the shell model, triangular (S3)¹ and quadrilateral (S4R)¹ elements. The solid pads on which the padeyes are attached, are meshed with solid hexahedral elements (C3D8R)¹. The solid elements are utilized in the model to avoid unnecessarily high stress concentrations around the area where the padeyes are attached. In order to gain a better estimation of where it exist in the model see Fig. 4.3 in next chapter. There are three translational and three rotational degrees of freedom (DOF) in each node [17], for the three elements shown in Fig. 2.1.



(a) *Triangular Elements.*

(b) *Quadrilateral Elements.*

(c) *Hexahedral Elements.*

Figure 2.1: *The three different types of elements used in the model.*

The beam model of the basket will be meshed with two different elements, linear (B31)² and quadratic elements (B32)², see Fig. 2.2. This is to compare the difference in collapse for the two mesh types, and to see what impact the two different meshes have on the results. The number of DOF for the linear and quadratic beam elements at each nodes is six. The element stiffness matrix \mathbf{K}_e is derived for a simple case without an effect of torsion and when the element is planar in App. B.3.



(a) *Linear beam element.*

(b) *Quadratic beam element.*

Figure 2.2: *The two element types used in the beam model.*

¹S3, S4R and C3D8R are Abaqus titles for denoting the linear elements

²B31 and B32 are Abaqus titles for denoting the linear and quadratic elements

2.2 Shell Structures

In the engineering field shell structures are frequently used in FE softwares since the simulation time is tremendously decreased compared to models meshed with solid elements. Shell structures come in various forms and shapes. It is important to know the behavior and performance of shell structures in order to use it properly. Shells in rotation describe the behavior in the best way and also minimizes the complexity in geometry [8]. Fig. 2.3 shows an example of how a shell structure can be composed [2].

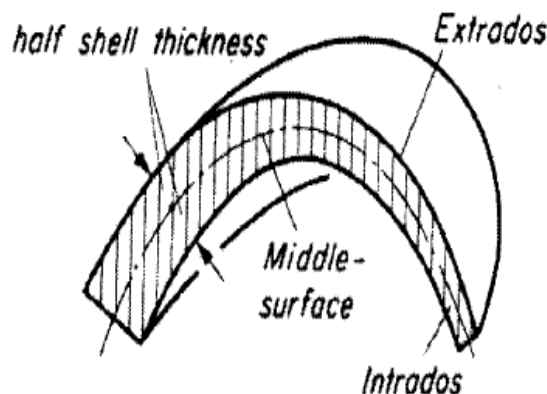


Figure 2.3: Geometrical representation of shell structure with mid surface and shell thickness

2.2.1 Shell Element Geometry

In Abaqus there are two types of shell elements available, conventional shell elements and continuum shell elements. The conventional shell elements discretize a reference surface by defining the elements plane (the geometry of the element), the surface normal and the curvature of the element. The nodes do not define the thickness of the shells. The thickness is defined in the section properties which is later applied to the corresponding shell. Continuum shell elements resemble a three-dimensional solid elements in that they discretize an entire three-dimensional body, but are formulated so that their kinematic and constitutive behavior is similar to conventional shell elements and not solid elements, according to Abaqus online manual [4]. The latter shell element mentioned is not used in this project since the necessity does not exist in discretizing an entire three-dimensional body.

2.2.2 Shell Thickness and Integration Points

The conventional shell elements in Abaqus must be assigned with a section consisting of a thickness, number of thickness integration points and a method of integration rule. The methods available in Abaqus are Simpson's integration rule and Gauss' integration rule. To verify which integration rule is the most appropriate in order to obtain an accurate result as possible, the study "Numerical Integration Strategy" conducted by Burgoyne and Crisfield [3] was used. Burgoyne and Crisfield studied different integration methods used in a plate and calculated the mean error by taking the difference between the numerical integration and the exact solution. This study concluded that the Gauss integration rule was the most accurate integration method since it resulted in less mean error than the other methods. In Fig. 2.4 the mean error versus integration points between two and thirteen are shown for the different integration rules.

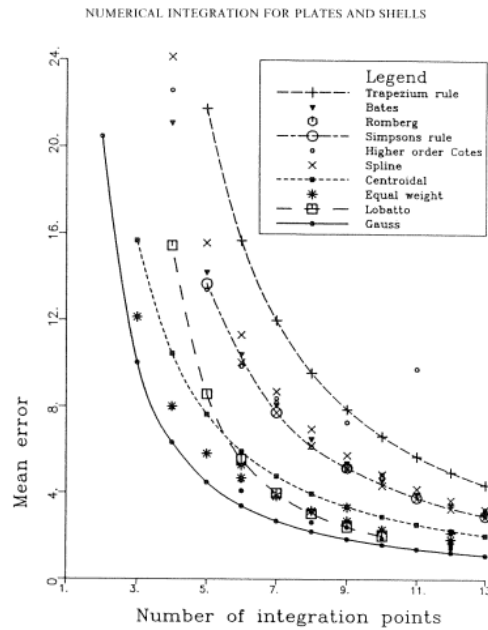


Figure 2.4: Mean error for different thickness integration methods.

In Abaqus the number of integration points must be odd because one point must be in the middle surface of the shell element. The default value for this number is five for homogeneous shells, which is sufficient for most non-linear problems. For linear problems three integration points are sufficient and will provide an exact integration through the thickness.

2.2.3 Thick and Thin Shells

Shell elements can be formulated as thin and thick. The thickness determines its shear behavior. Thickness to length ratio is used to define if a shell element is thick or thin according to the Abaqus online documentation ???. A shell is considered "thick" if the ratio is greater than 1/15 and if it is less than 1/15 it is considered as "thin". If the shell is thick the transverse shear deformation is taken into account and is an important factor, while a thin shell is neglecting the shear deformation due to a thickness that is small enough to be ignored. Fig. 2.5 shows the transverse shell deformation for a thin and a thick shell.

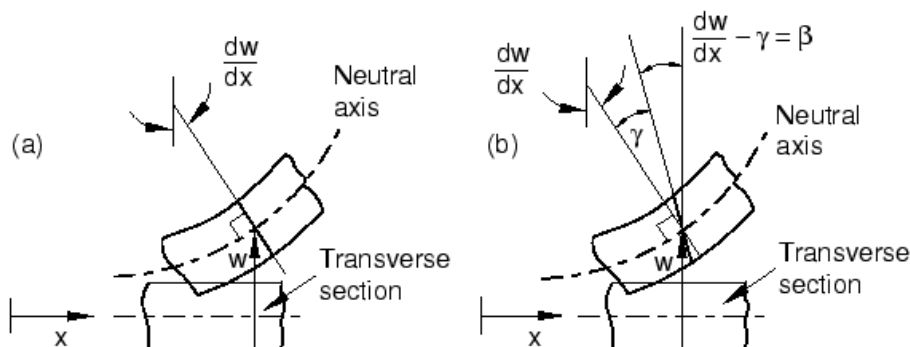


Figure 2.5: Transverse shell deformation of thin (a) and thick (b) shells.

The basket is in this case modelled as a thin shell since the length of the geometry is large compared to its thickness. In the FE software Abaqus a thin shell model uses the kinematics of Kirchhoff theory, see App. A to gain the general principles of Kirchhoff's plate theory.

2.3 Beam Structures

Beam structures are traditionally used for civil engineering structural elements and for buildings but it is also used in small structures as machine frames or other mechanical components. The structural element beam is characterized by its cross section, its length and its material. A beam is capable of taking up loads by resisting bending. When these loads are applied to the beam structure it induces a bending moment.

The finite element software Abaqus offers a set of beam elements. A beam element is defined as an element in which the assumptions are made so that the mathematical solution to the problem is reduced to one dimension. In order to make this assumption reasonable the beam must be a continuum. [4]

In this case the beam elements applied to the basket is using the kinematic of Timoshenko's theory.

2.3.1 Timoshenko Beam Theory

The classical Euler-Bernoulli beam theory approach is the simplest one and it is based in the kinematic assumption of straight lines transverse to the beam's axis remain straight, and undistorted after deformation i.e they do not extend and they will always remain normal to the mid-plane of the beam. Timoshenko beam theory, on the other hand is including the "transverse shear strain" in which the cross section may not necessarily remain normal to the beam axis. [6]

The displacement vector for a Timoshenko beam has the following components of the vector $\mathbf{u} = [u \ v \ w]$ and it can be written as

$$u(x, z) = -z\phi(x), \quad v = 0, \quad w(x, z) \quad (2.2)$$

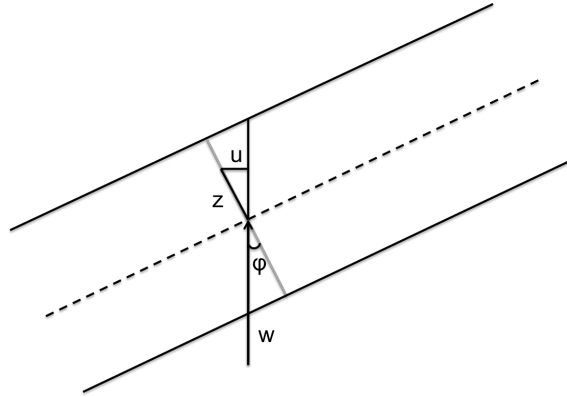


Figure 2.6: Deformation of a Timoshenko beam.

The strains can then be computed as

$$\epsilon_{xx} = \frac{\partial u}{\partial x} = -z\phi', \quad \gamma_{xz} = 2\epsilon_{xz} = \frac{\partial u}{\partial z} + \frac{\partial w}{\partial x} = -\phi + w' \quad (2.3)$$

The corresponding virtual strains are

$$\delta\epsilon_{xx} = -z\delta\phi', \quad \delta\gamma_{xz} = -\delta\phi + \delta w' \quad (2.4)$$

The internal shear force, V and bending moment, M are

$$M = \int_A \sigma_{xx} z dA, \quad V = \int_A \sigma_{xz} dA \quad (2.5)$$

In order to compensate the difference between the actual shear force and the shear force from the Timoshenko beam theory, a correction factor K_s is introduced in Eq. (2.7). The shear correction factor is defined in different ways and Timoshenko (1992) developed the frequency-matching approach. By equating the frequency of vibration using plane stress equations of elasticity. [10]

The shear correction factor is calculated as

$$K_s = \frac{5(1 + \nu)}{6 + 5\nu} \quad (2.6)$$

Linear elasticity assumption with shear modulus G and Young's modulus E gives

$$V = K_s \int_A \sigma_{xz} dA = K_s \int_A G(-\phi + w') dA = GK_s A(-\phi + w'), \quad M = \int_A \sigma_{xx} z dA = -EI\phi' \quad (2.7)$$

The internal virtual work is

$$\delta W_{int} = \int_{\Omega} \sigma_{ij} \delta \epsilon_{ij} d\Omega = \int_0^L \int_A \sigma_{xx} \delta \epsilon_{xx} + \sigma_{xz} \delta \gamma_{xz} dA dx \quad (2.8)$$

The external virtual energy δW_{ext} is as (without any end loads acting on the beam)

$$\delta W_{ext} = \int_0^L q \delta w dx \quad (2.9)$$

The internal virtual *power* then becomes

$$\begin{aligned} \delta W_{int} + \delta W_{ext} &= \int_0^L M(-\delta\phi') + V(-\delta\phi + \delta w') - q\delta w dx \\ &= -[M\delta\phi]_0^L \int_0^L (-V + M')\delta\phi dx + [V\delta w]_0^L - \int_0^L (V' + q)\delta w dx = 0 \end{aligned} \quad (2.10)$$

The equilibrium equations for a Timoshenko beam are

$$\begin{aligned} -V + M' &= 0 \\ V' + q &= 0 \end{aligned} \quad (2.11)$$

By using the definitions of V and M by Hooke's law, Eq. (2.11) can be rewritten in terms of ϕ and w as

$$\begin{aligned} GK_s A(\phi - w') - EI\phi'' &= 0 \\ GK_s A(-\phi' + w'') + q &= 0 \end{aligned} \quad (2.12)$$

By combining Eq. (2.12) the differential equation in terms of ϕ becomes

$$EI\phi''' = q \quad (2.13)$$

And w can be computed from

$$w' = \frac{-EI}{GK_s A} \phi'' + \phi \quad (2.14)$$

The complete BCs are also obtained from the principle of virtual power

$$\begin{aligned} \delta\phi = 0 \quad \text{or} \quad M = 0 \quad \text{for} \quad x = 0 \quad \text{and} \quad x = L \\ \delta w = 0 \quad \text{or} \quad V = 0 \quad \text{for} \quad x = 0 \quad \text{and} \quad x = L \end{aligned}$$

2.4 Material Model

When a material has been exposed to enough applied force it will begin to change its shape. This is called deformation. When the force has been removed and if the material has recovered to its original shape, the material has experienced elastic deformation. On micro level this means that the atoms have experienced stretching of the bond, but there has been no grain boundary slip. When the applied force on the material is great enough and the material does not recover to its original shape it has experienced plastic deformation which is permanent. This means that there has been a slip between grain boundaries on microscopic level.

2.4.1 Elastic-plastic Material Model

The simplest type of plasticity model is an isotropic, perfectly elasto-plastic material associated with a flow rule. It is realistic only under certain conditions and should be used with caution. The rheological model for perfectly plastic behavior can be seen in Fig. 2.7 where it behaves elastically and then perfectly plastic.

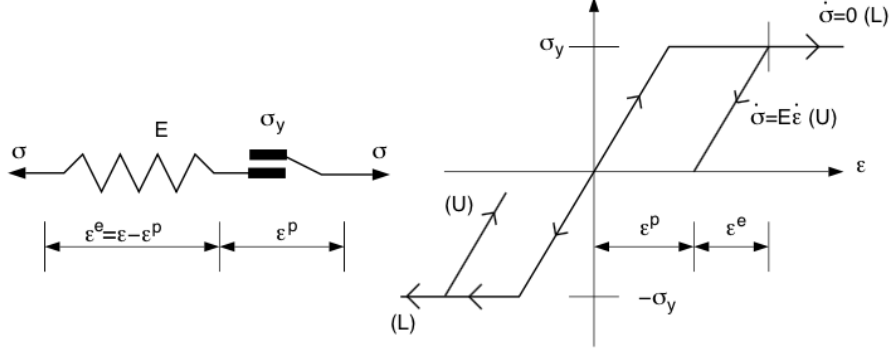


Figure 2.7: *Prototype rheological model for elastic perfectly plastic behavior and stress-strain relationship.*

The free energy for a 1D stress-strain state is defined as,

$$\Psi = \frac{1}{2}E(\epsilon^e)^2 = \frac{1}{2}E(\epsilon - \epsilon^P)^2 \quad (2.15)$$

Where E is the elastic modulus and $\epsilon^e = \epsilon - \epsilon^P$ is the elastic spring from Hooke's law. The constitutive equation for the stress is then,

$$\sigma = \frac{\partial \Psi}{\partial \epsilon} = E(\epsilon - \epsilon^P) \quad (2.16)$$

The dissipative stress, σ^P conjugated to ϵ^P is then,

$$\sigma^P = -\frac{\partial \Psi}{\partial \epsilon^P} = E(\epsilon - \epsilon^P) \equiv \sigma \quad (2.17)$$

The yield criterion is $\Phi = 0$, where Φ is chosen as

$$\Phi(\sigma) = |\sigma| - \sigma_y \quad (2.18)$$

For this simple prototype model the magnitude of stress can never exceed the yield stress and therefore the admissible stresses are defined as those which are $\Phi \leq 0$. Plastic strain may be produced when $\Phi = 0$ and the constitutive rate equation for ϵ^P is then formulated as the associative flow rule

$$\dot{\epsilon}^P = \lambda \frac{\partial \Phi}{\partial \sigma} = \lambda \frac{\sigma}{|\sigma|} \quad (2.19)$$

where λ is the plastic multiplier and is always a positive scalar variable. By combining Eq. 2.19 and 2.16 the differential equation for the stress is obtained as

$$\dot{\sigma} = E\dot{\epsilon} - \lambda E \frac{\sigma}{|\sigma|} \quad (2.20)$$

This formulation is complemented by the elastic-plastic loading criteria. Loading criteria follows,

$$\lambda \geq 0, \quad \Phi(\sigma) \leq 0, \quad \lambda \Phi(\sigma) = 0 \quad (2.21)$$

2.4.2 Hardening Plastic Behavior

When a "hardening spring" with stiffness H related to the plastic strain is inserted in the rheological model it illustrates the behavior of hardening plasticity according to M.Jirásek and Z.P. Bezant. [11] and Kenneth Runesson. [16] as showed in Fig. 2.8

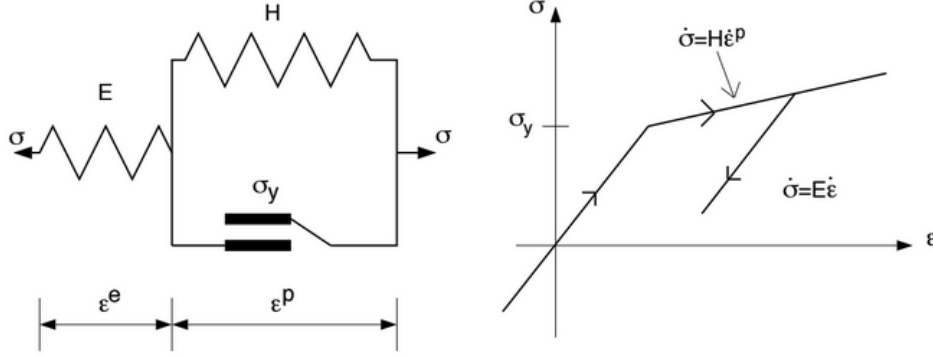


Figure 2.8: *Prototype rheological model for elastic-hardening-plastic material and stress-strain relationship.*

The isotropic hardening variable k is introduced and the free energy becomes,

$$\Psi = \frac{1}{2}E(\epsilon - \epsilon^P)^2 + \frac{1}{2}Hk^2 \quad (2.22)$$

The stress then becomes,

$$\sigma = \frac{\partial \Psi}{\partial \epsilon} = E(\epsilon - \epsilon^P) \quad (2.23)$$

$$\sigma^P = -\frac{\partial \Psi}{\partial \epsilon^P} \equiv \sigma \quad (2.24)$$

The dissipative stress κ , also denoted as the "drag stress" is associated with k , is given as

$$\kappa = -\frac{\partial \Psi}{\partial k} = -Hk \quad (2.25)$$

The yield function is now defined as

$$\Phi(\sigma, \kappa) = |\sigma| - \sigma_y - \kappa \quad (2.26)$$

Inelastic deformation can be produced when $\Phi = 0$. The associative flow and hardening rule are then defined as

$$\dot{\epsilon}^P = \lambda \frac{\partial \Phi}{\partial \sigma} = \lambda \frac{\sigma}{|\sigma|} \quad (2.27)$$

$$\dot{k} = \lambda \frac{\partial \Phi}{\partial \kappa} = -\lambda \quad (2.28)$$

The plastic multiplier, λ is still defined by the loading criteria presented in Eq. (2.21). The dissipative stress rate, $\dot{\kappa}$ can also be obtained by differentiating Eq. (2.25) and combining it with Eq. (2.28). One obtain the following set of equations

$$E\dot{\epsilon} = E\dot{\epsilon} - \lambda E \frac{\sigma}{|\sigma|} \quad (2.29)$$

$$\dot{\kappa} = H\lambda \quad (2.30)$$

which are subjected to the following loading criteria

$$\lambda \geq 0, \quad \Phi(\sigma, \kappa) \leq 0, \quad \lambda \Phi(\sigma, \kappa) = 0 \quad (2.31)$$

Elastic-plastic tangent stiffness modulus is defined as

$$E^{ep} = \left(1 - \frac{E}{h}\right), \quad E = \frac{E}{h}H \quad (2.32)$$

The following situations are distinguished with a generalization of the hardening concept. [11], [16]

$$\begin{aligned} \text{Hardening : } & H > 0 \Rightarrow E^{ep} > 0, \quad (\dot{\kappa} > 0) \\ \text{PerfectPlasticity : } & H = 0 \Rightarrow E^{ep} = 0, \quad (\dot{\kappa} = 0) \\ \text{Softening : } & H < 0 \Rightarrow E^{ep} < 0, \quad (\dot{\kappa} < 0) \end{aligned} \quad (2.33)$$

2.5 Newton's Method

For nonlinear problems, it is not possible to solve all the components in the displacement vector \mathbf{a} explicitly. Therefore an iterative technique is necessary until convergence has been reached. The iterative method used in this project is Newton's method. It is great at solving nonlinear equations due to solving it implicitly and it updates the Jacobian at each iterative step. In order to get a deep understanding of which of the components in the displacement vector that needs to be solved by this iterative technique, the "Non-linear Finite Element Analysis" written by Fredrik Larsson can be examined [12]. In order to derive this method an arbitrary residual function is chosen, see Eq. (2.34) with the Jacobian matrix \mathbf{J} Eq. (2.35).

$$\mathbf{g}(\mathbf{x}) = \mathbf{0} \quad (2.34)$$

$$\mathbf{J} = \frac{d\mathbf{g}}{d\mathbf{x}} = \begin{bmatrix} \frac{\partial g_1}{\partial x_1} & \frac{\partial g_1}{\partial x_2} & \cdot & \frac{\partial g_1}{\partial x_{Nfree}} \\ \frac{\partial g_2}{\partial x_1} & \frac{\partial g_2}{\partial x_2} & \cdot & \frac{\partial g_2}{\partial x_{Nfree}} \\ \cdot & \cdot & \cdot & \cdot \\ \frac{\partial g_{Nfree}}{\partial x_1} & \frac{\partial g_{Nfree}}{\partial x_2} & \cdot & \frac{\partial g_{Nfree}}{\partial x_{Nfree}} \end{bmatrix} \quad (2.35)$$

The method starts with a guess solution at \mathbf{x}^k . By linearizing the Eq. (2.34) around the guess solution point, a Taylor series approximation can be obtained.

$$\mathbf{g}(\mathbf{x}^k + \Delta\mathbf{x}^k) = \mathbf{g}(\mathbf{x}^k) + \mathbf{J}(\mathbf{x}^k)\Delta\mathbf{x}^k + O((\Delta\mathbf{x}^k)^2) \approx \mathbf{g}(\mathbf{x}^k) + \mathbf{J}(\mathbf{x}^k)\Delta\mathbf{x}^k \quad (2.36)$$

And letting the updated guess be $\mathbf{x}^{(k+1)} = \mathbf{x}^k + \Delta\mathbf{x}$ and aiming for the solution $\mathbf{g}(\mathbf{x}^{(k+1)}) = \mathbf{0}$. The linear approximation from Eq. (2.36) can be used to get the updated \mathbf{J} and \mathbf{x} for each iteration.

$$\begin{aligned} \mathbf{J}(\mathbf{x}^k)\Delta\mathbf{x}^k &= -\mathbf{g}(\mathbf{x}^k) \\ \mathbf{x}^{(k+1)} &= \mathbf{x}^{(k)} + \Delta\mathbf{x}^k \end{aligned} \quad (2.37)$$

The convergence of this method is quadratic, i.e.

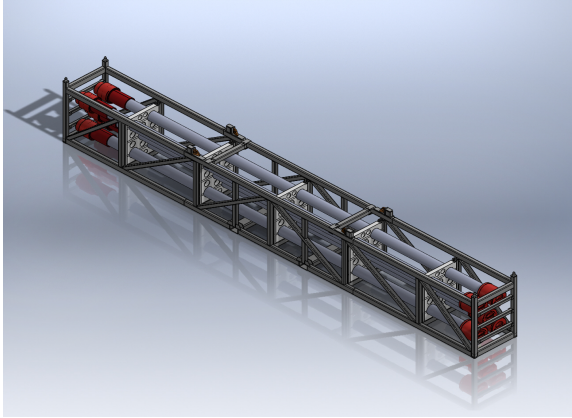
$$|\mathbf{x} - \mathbf{x}^{(k+1)}| \leq C |\mathbf{x} - \mathbf{x}^{(k)}|^2 \quad (2.38)$$

3 Finite Element Representation of PO unit

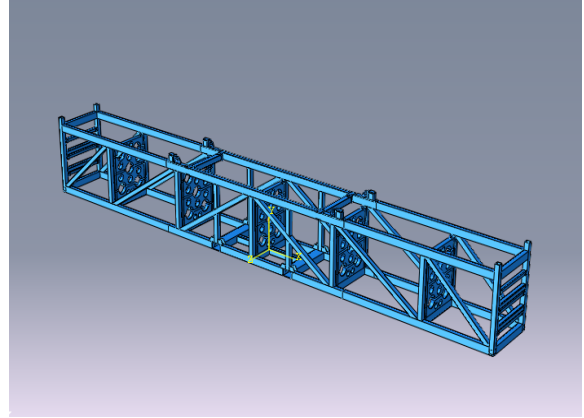
In order to proceed with the analyses some basic requirements are necessary which will be presented and illustrated in the following chapter. The content of this chapter will firstly describe the geometry of the PO unit and how it is defined according to the offshore standard. Further the material properties for the basket will be described and lastly the definition of the acceptance criteria will be denoted.

3.1 Geometry

The geometry of the PO unit is a rectangular shaped basket with an approximate length and width of 12 and 1 meters respectively. The basket is used for transporting the five risers, each with a weight of 2200 kg. In Fig. 3.1 (a) the PO unit can be seen together with the five risers inside (payload). Fig. 3.1 (b) is showing the provided 3D CAD model from Aker Solutions. The CAD model did not come with the risers in it therefore the load will be distributed to the frames where the risers are supported. It consists of several parts such as hollowed beams, padeyes, screw nuts etc, see Fig. 3.2 (a) and (b)

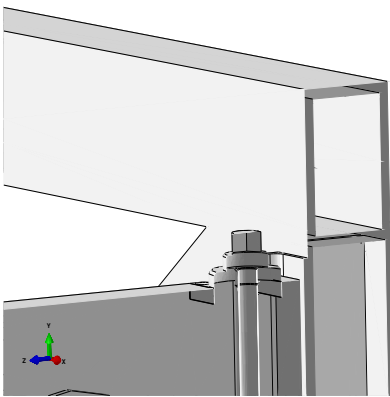


(a) Illustration of the PO unit

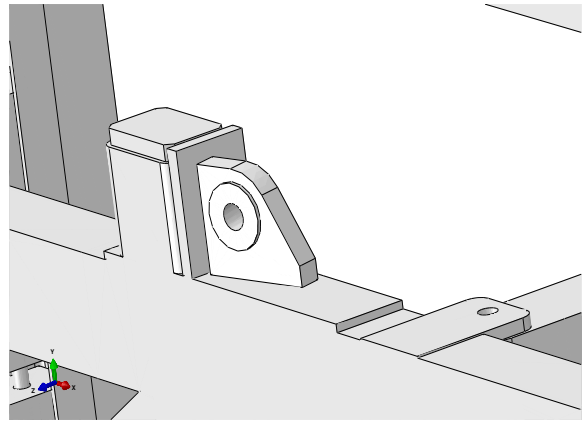


(b) The provided CAD model

Figure 3.1: Illustration of the basket with the risers in (a) and without the risers as a CAD model in (b)



(a) Section cut to illustrate the hollow beams.



(b) Original shape of the padeye.

Figure 3.2: The hollow beams and the padeye are showed which are parts of the basket.

The basket consists of primary and secondary structure and are shown in Fig. 3.3. The *primary structure* is defined according to the standard [1] as the load bearing structure e.g the frame of the basket, global structural strength parts, lifting points (padeyes) seen in Fig. 3.2 (b) etc. The primary structure must be included in the calculations since they are load bearing and influences the results. It is though approved to simplify the primary

structure. The padeyes or the so called lifting points were simplified as a point in order to save unnecessary computation time of solid elements. The *secondary structure* contains the parts that are not load bearing, e.g. frames, protection structures, etc. These parts or components can be removed from the calculation but the mass of the removed parts or components must be implemented in the calculation model as nonstructural masses.

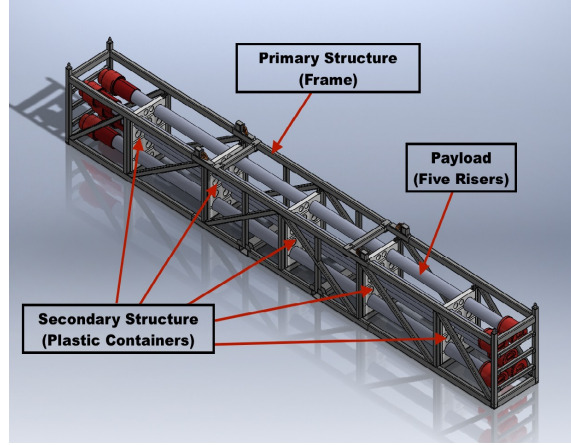


Figure 3.3: Basket containing primary structure, secondary structure and payload.

The information about the PO unit has mostly been defined from the industrial offshore standard DNV 2.7-3 [1]. In order to select an operational class for the PO unit some crucial information is needed, such as the purpose of the unit and the load case. This is to determine the acceptance criterion which is described in Sec. 3.3. First the PO unit type must be known, which in this case is A. Type A stands for a PO unit which consists with a primary structure frame and is used for service packages such as, pumps, risers, generation units, pressure vessels, skid mounted manifolds or process arrangements of portable nature. Estimates of the masses for primary structure, secondary structure and the payload was taken from the 3D CAD model. *Tare mass* is the total mass of primary and secondary structures. Mass gross weight (MGW) is the total mass of the PO unit including the payload. MGW decides the operational class, see Tab. 3.1.

Table 3.1: PO unit information

PO unit type	A
Primary Structure	3.50 tons
Secondary Structure	$0.59 \approx 0.70$ tons
Payload	11 tons
Operational Class	DNV 2.7-3 R60

The primary structure consist of all the frames of the basket while the secondary structure are those who supports the risers (plastic containers). The plastic containers can be seen in Fig. 3.1 (a) and a rough estimate of the mass was made, which in turn gave a weight of 0.7 tons.

Table 3.2: Mass estimates and contingencies for the basket.

	Estimated mass [tons]		Mass used in simulations [tons]		Contingency factor	
	Shell	Beam	Shell	Beam	Shell	Beam
Tare mass	$0.7 + 3.5 = 4.2$	$3.12 + 0.7 = 3.82$	4.47	4.48	1.07	1.17
Payload	$2.2 \times 5 = 11$	$2.2 \times 5 = 11$	11.7	11.7	1.06	1.06
MGW	$4.2 + 11 = 15.2$	$3.82 + 11 = 14.82$	16.17	16.18	1.06	1.09

3.2 Material Properties

The next step consisted of applying the material to the basket. Depending on the thicknesses for the different parts of the basket the plasticity properties differed. The material applied to the calculation models is EN 10025 S355, see App. C, and is illustrated in Fig. 3.4 where the stress-strain relationship can be seen for this material. The material is of a multi-linear elastic-plastic model with kinematic hardening up to 0.2 % and then it becomes perfectly plastic. This material model is following the same principles discussed in Sec. 2.4. All the thicknesses for the different parts of the basket, were below 16 mm and therefore the same material properties were applied to the whole model. For more detailed information about the material properties, see App. C where the plasticity properties are shown for a thickness value below 16 mm.

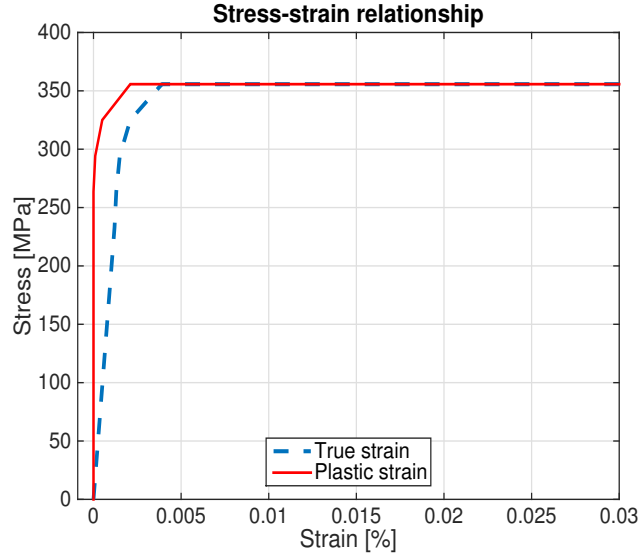


Figure 3.4: *Plastic and true strain properties for the material S355.*

Table 3.3: Material properties.

Material	Young's Modulus [GPa]	Poisson's ratio	Yield stress [MPa]	Density [tons/mm ³]
EN 10025 S355	202,35	0.3	355.7	7.75×10^{-9}

3.3 Acceptance Criteria

The interesting result for the lift case is the ultimate capacity (collapse load). The collapse load F_{RK} , has two definitions according to the the industrial offshore standard DNV 2.7-3 [1]

Collapse occurs when:

1. the least of the load corresponding to the last converged increment. This definition is considering the collapse at the last linear part of the structural response. This can be hard to verify since it is difficult to visualize the last converged increment and therefore the second way of defining the collapse has been utilized.
2. the structural response stiffness is reduced with 1/3 of the initial stiffness.

Let us consider the case where a gravity load is applied to the model and the response obtained is the displacement, see Fig. 3.5. The displacement is measured at a point where the material has yielded and where the plastic strain is sufficiently high compared to the rest of the model. Hence, the displacement should not be measured at a place where stress concentration exist, e.g at sharp edges, or corners. The initial stiffness is obtained by calculating the gradient in the elastic area of the response.

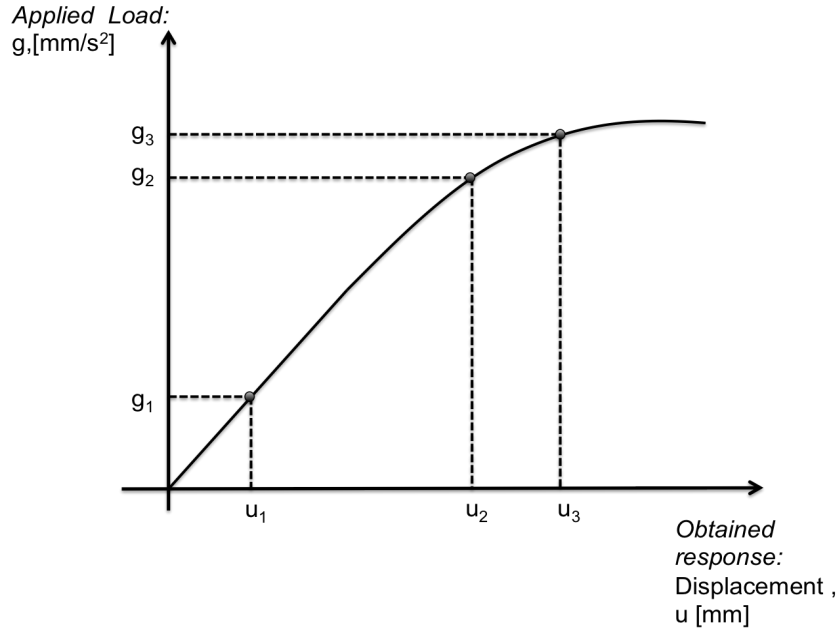


Figure 3.5: Load-displacement curve

The initial stiffness response is calculated as in Eq. (3.1).

$$\frac{\Delta g^1}{\Delta u^1} = \frac{g_2 - g_1}{u_2 - u_1} = \{\text{Let us assume a reasonable value}\} = 2.0 \quad (3.1)$$

Then 1/3 of the initial stiffness must be checked

$$\frac{\Delta g^1}{\Delta u^1} \frac{1}{3} = \frac{2}{3} \quad (3.2)$$

Gradient between point 2 and 3 is then calculated as

$$\frac{\Delta g^2}{\Delta u^2} = \frac{g_3 - g_2}{u_3 - u_2} = \{\text{Let us assume a reasonable value here as well}\} = 1.3 \quad (3.3)$$

$$\frac{\Delta g^1}{\Delta u^1} - \frac{\Delta g^2}{\Delta u^2} = 2.0 - 1.3 = 0.7 > \frac{2}{3} \rightarrow \text{Collapse!} \quad (3.4)$$

Collapse has occurred since the gradient has reduced with more than 1/3 of the initial stiffness gradient. In this project the collapse was calculated in MATLAB.

Collapse Load

The collapse load, F_{Rk} is determined by Eq. (3.5).

$$F_{Rk} = MGW \times c \times g \quad (3.5)$$

where MGW is the mass gross weight, c is the measured gravity multiplier at the collapse occurrence and g is the gravity.

4 FE Analysis of Normal Lift

In this section the FE analysis of a "normal lift" will be discussed of the PO unit. The normal lift case is when the basket is initially hanging still in the air with zero gravity. When the simulation starts the gravity is introduced and gradually increased which will simulate an increase in mass for the basket in reality. The finite element analysis are based on a limit analysis, i.e the load is increased to either structural instability or until a numerical divergence occurs. The normal lifting analysis will be following the standard DNV 2.7-3 [1].

4.1 Methodology in Abaqus CAE

With the 3D solid CAD model received from Aker Solutions, the shell model could be constructed in the "part" module as midsurfaces from the solid CAD model. Simplifications to the geometry were made in order to obtain the final calculation models. The beam model was constructed simply by measuring the geometry of the solid CAD model and creating a wireframe with those measurements. The wireframe was inserted with a box-shaped profile with lengths and thicknesses of the cross section. The material was then applied to the cross sections. Reference points were created where point masses could be attached, which was connected to the model with the help of coupling constraints which couples the mass to the model. The model was connected with rigid wires in the padeyes to the master link (ML) which gave the hanging effect of the basket, see Fig. 4.1. The ML was locked in the translational and rotational DOFs. The mass of the risers was applied on the model in two different ways, uniformly from the riser's center of mass (COM) and by manually calculating the fraction of the mass that would rest on each support analytically. When the model setup was complete a gravity load was added and gradually increased during the simulation.

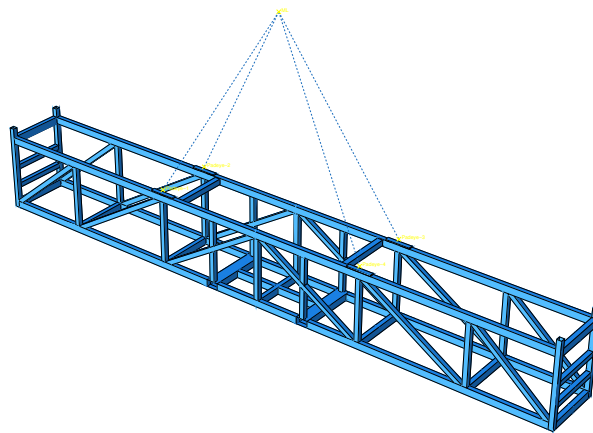
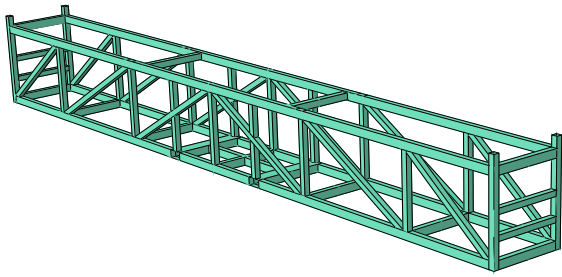


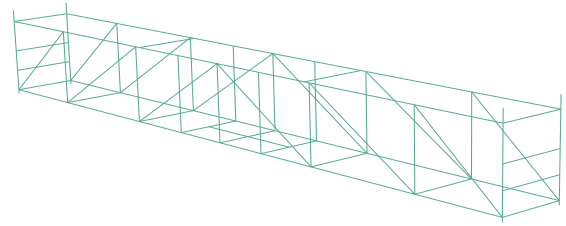
Figure 4.1: Wires connected from the master link to the padeyes

4.1.1 Model Simplifications

The 3D CAD model that was received from Aker and imported into Abaqus, where a few simplifications were made. The secondary structure that can be seen in Fig. 3.3 was removed. Midsurfaces were created from the solid hollow beams to construct the *shell model*. The solid parts were then removed and only the midsurfaces remained. At this point there existed a few gaps in the model where there were no surfaces. These gaps were extruded in order to make the model complete. The *beam model* was made as a wireframe with the same geometry as the shell model, with a box shaped cross section applied to it. Fig. 4.2 shows the two calculation models that was used in the FE analysis.



(a) *Shell calculation model.*



(b) *Beam calculation model.*

Figure 4.2: *Simplified calculation models.*

Due to the conventional shell elements being used in the model, there will be a significantly high stress concentration in close proximity to where the padeye is constrained with coupling constraint. To avoid this a solid pad was added into the model where the padeye constraint could be connected to instead, see Fig. 4.3. When this was added into the model the stress concentration was distributed on the solid pads instead. The reason for this is that

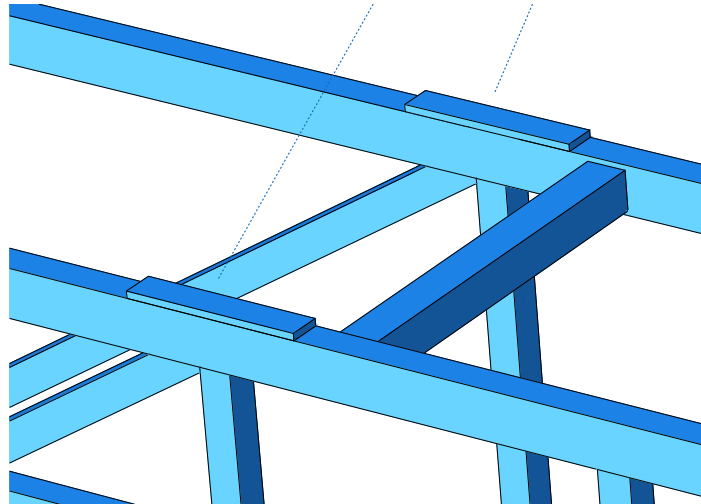


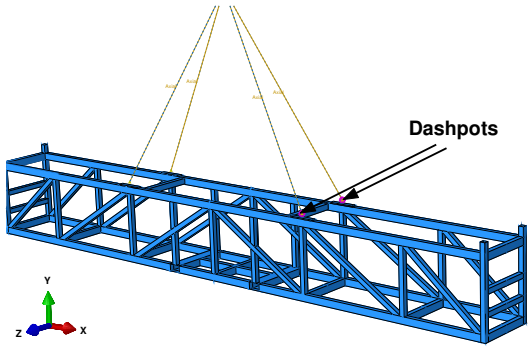
Figure 4.3: *Solid pads added to shell model.*

4.1.2 Model Setup

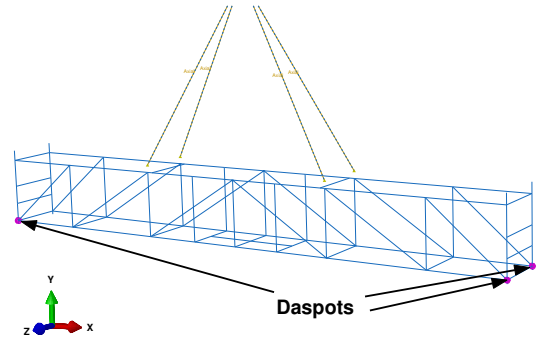
In the following section, the settings to complete the final models for analysis are explained in detail. The constraints and the loading procedure will be presented for the normal lift case.

Dashpots

When the basket is lifted it will tilt due to an unsymmetrical riser weight distribution. In order to get a more stable simulation, dashpots were used to stabilize the movement of the basket. These dashpots were connected to the ground which can be seen in Fig. 4.1. There should be at least two dashpots connected to the model to restrict the motion in X and Z direction. If no dashpots are applied to the basket the basket starts to rotate unrealistically much and will not give a proper motion of a lifting procedure.



(a) Dashpots placed at the padeyes on the shell structure.



(b) Dashpots placed at the corners on the beam model.

Figure 4.4: Dashpots applied to the shell and the beam model.

In the Fig. 4.1 the dashpots are applied in different places to the models. According to the standard DNV [1] the dashpots should be applied onto the padeyes but due to instability in motion of the beam model, the dashpots were applied onto the basket in order to stable the motion.

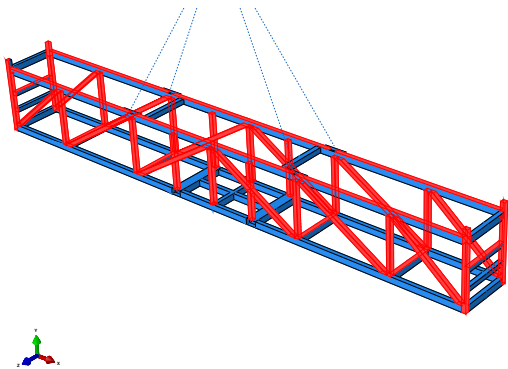
The dashpot coefficient was calculated with the help of Eq. (4.1)

$$c = 0.01 \frac{FT}{L} \quad (4.1)$$

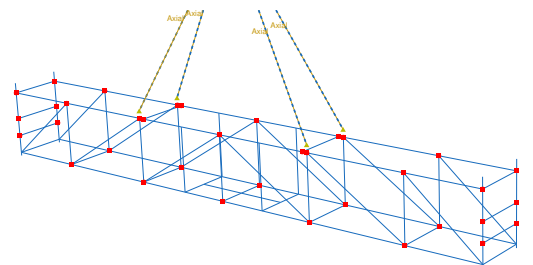
where c is the dashpot coefficient, F is the design lifting force in the master node where the wires are connected, T is the time period of a step and L is a characteristic dimension of the PO unit (the greatest is chosen). The definition of the dashpot coefficient is taken from the standard DNV [1].

Nonstructural mass

Simplifications of the models will contribute to less mass than it had originally which means that the removed material must be reapplied to make the model's properties as similar as the 3D CAD model. This was done by applying nonstructural masses. When the model was "cleaned" and the material was removed, the center of mass was most likely changed. It was important to make sure that the position of center of mass remained at same location after applying the nonstructural mass as it was for the 3D CAD model. When the nonstructural mass was applied, it was placed so the center of mass would change back to where it was in the original model. The nonstructural mass was applied to the surfaces on the shell model as can be seen in Fig. 4.5 (a). The beam model was applied with nonstructural point masses at the connection points and can be seen in Fig. 4.5 (b).



(a) Nonstructural mass applied to the surfaces on the shell structure



(b) Nonstructural mass placed at the points on the beam model

Figure 4.5: Nonstructural masses applied to the shell and beam model in order to make it conservative

Riser weight distribution

The weight of the risers was implemented into the model in two different ways. First as a point mass which was constrained to the five supports (uniform distribution). The second way was to calculate the fraction of the mass acting on the five support analytically using the secondary software "GoBeam" (manual distribution), see App. D.

Riser weight - Uniform distribution

The first way of implementing the riser weight into the model was to add it as a point mass in the location where the COM for the riser is. The mass added was 11.7 tons, 11 tons from the riser and then an additional 0.7 tons in order to be conservative. This point mass was constrained to the five supports with the constraint "Continuum distributing". For more information about this constraint see Sec. 4.1.3. This implementation can be seen in Fig. 4.6 and Fig. 4.7.

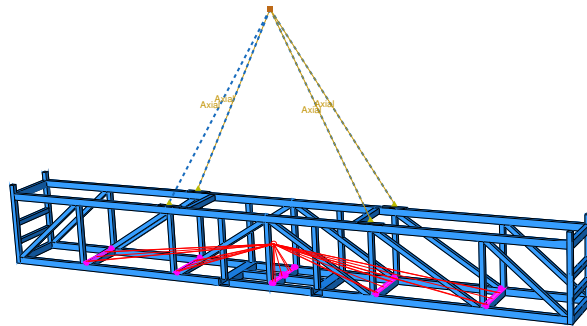


Figure 4.6: *Uniform distribution of the riser mass by using the constraint "Continuum distributing coupling" in Abaqus.*

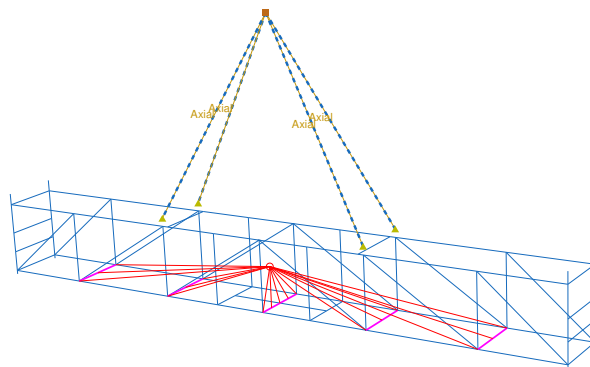


Figure 4.7: *Uniform distribution of the riser mass by using the constraint "Continuum distributing coupling" in Abaqus.*

Riser weight - Manual distribution

When constraining the riser mass to the model there was not a sufficiently good option in Abaqus. The weight from the risers should be applied as can be seen in Fig. 4.8. In this loadcase a portion of the mass of the riser is outside the supports. When the mass is distributed to the five support in the uniform loadcase it will not take this into consideration.

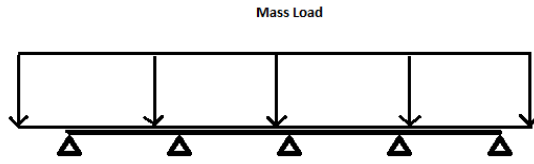


Figure 4.8: *Uniform load.*

So a more sophisticated approach was to add the contribution the weight of the riser would have on each support individually. In order to determine the distribution of the mass a third party excel document was used, see App. D. In this document the load, geometry, inertia of the beam (risers in this case) and spring constant must be specified. Here the supports are considered as springs, because in theory the supports act as stiff springs. The spring constants were calculated by clamping the padeyes and applying a force of 1 kN on each support. The displacement on each support was extracted from the simulation and used in Eq. (4.2) to get the spring constants.

$$F = kx \quad (4.2)$$

The distribution of the reaction force acting on each support is shown in Fig. 4.9. With the help of these results the fraction of the riser mass could be determined and applied for each support in the beam and shell model, see Tab. 4.1.

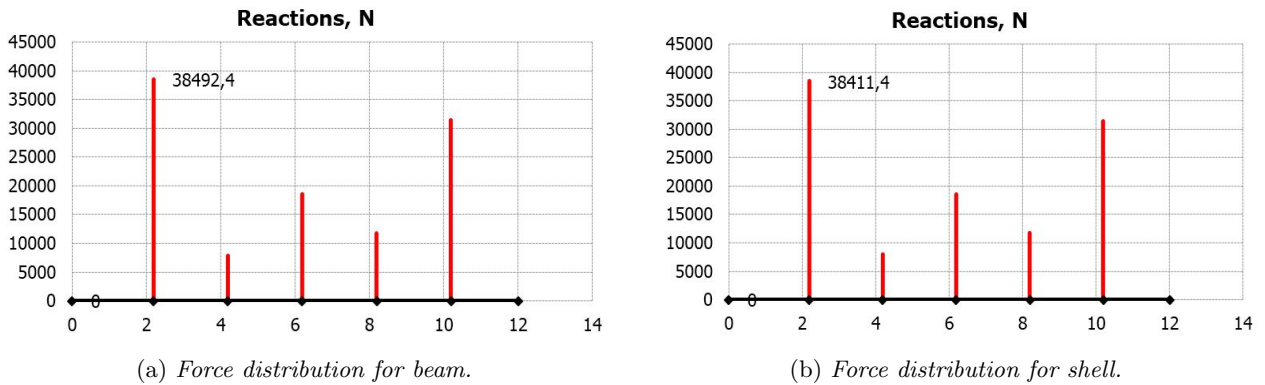


Figure 4.9: *Reaction forces on each support the beam and shell model.*

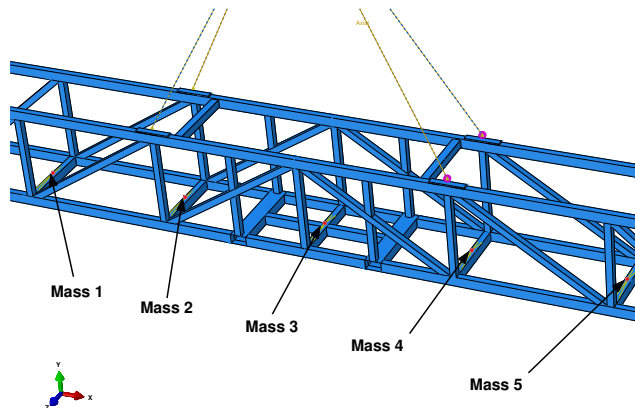


Figure 4.10: *Riser weight distribution of the shell calculation model.*

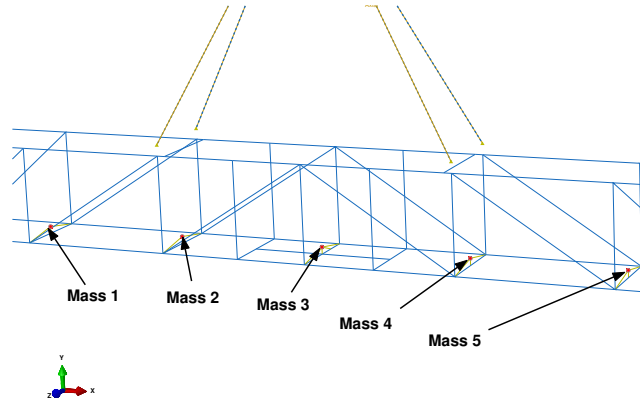


Figure 4.11: Riser weight distribution of the beam calculation model.

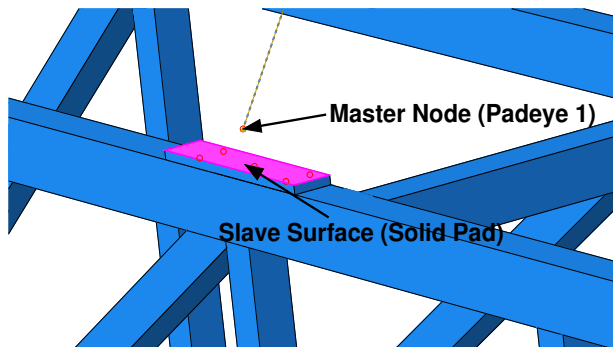
Table 4.1: Mass distribution of the supports from left to right.

	Mass 1 [tons]	Mass 2 [tons]	Mass 3 [tons]	Mass 4 [tons]	Mass 5 [tons]
Shell model	4.2	0.9	2.0	1.3	3.4
Beam model	4.2	0.8	2.0	1.3	3.4

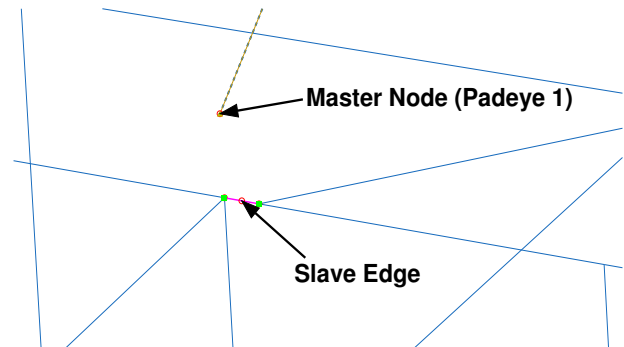
4.1.3 Constraints

In Abaqus two constraints, tie and coupling were applied to the models. The constraints in Abaqus have the purpose to connect different parts of the structure. The constraints partially or fully eliminate DOF of a group of nodes and couple their motion to the motion of a master node (or nodes).

- **Tie** - This is a simple constraint that connects two different surfaces or adjacent nodes. It will not matter if one is a surface from a shell and the other a surface from a solid. This is why it was chosen to constraint the solid pads onto the shell model.



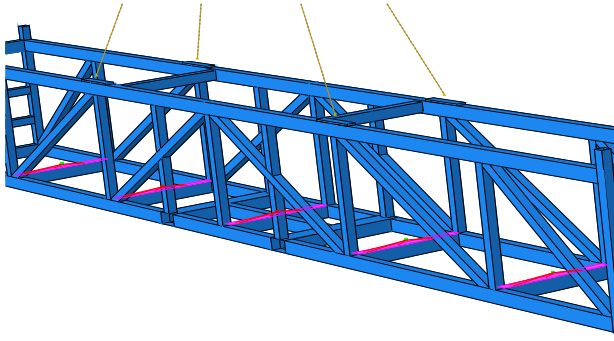
(a) Tie constraint illustrating the master node (padeye 1) and the slave surface (solid pad).



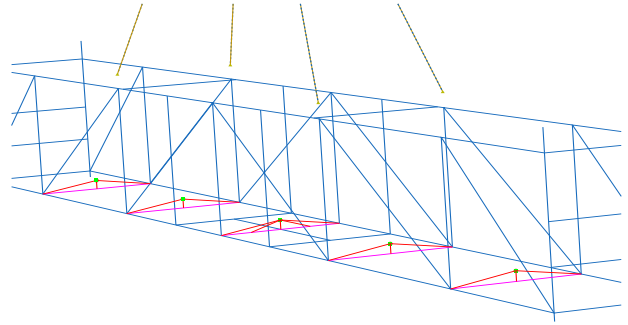
(b) Tie constraint illustrating the master node (padeye 1) and the slave edge at the primary structure.

Figure 4.12: The calculation models showing the tie constraints, (a) shows the shell model and (b) shows the beam model.

- **Coupling** - A master node and a slave surface can be coupled to each other using either continuum- or structural distributions. Continuum distribution, couples the displacement and rotation of each fastening point with the average displacement of the nodes in a surrounding slave area. When constraining the mass onto the supports the continuum distribution was used, see Fig. 4.13.



(a) Coupling constraint to fasten the masses onto the supports in the shell model.



(b) Coupling constraint to fasten the masses onto the supports in the beam model.

Figure 4.13: Coupling constraint.

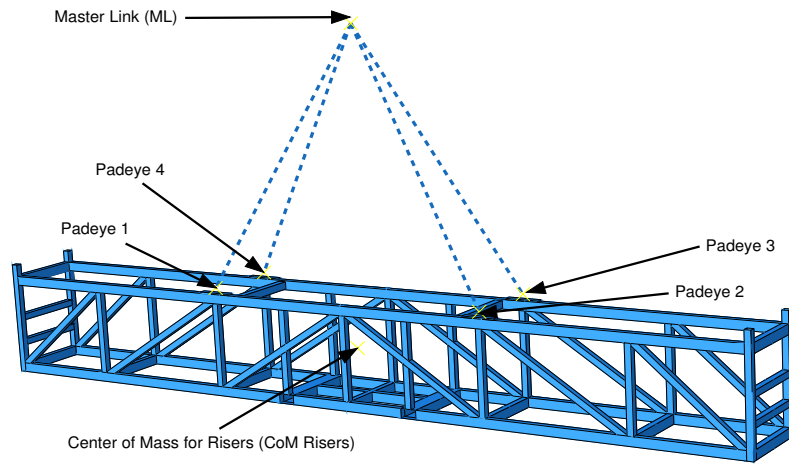
4.1.4 Boundary Conditions and Load

In this case there were two BCs. The first BC locks the master link (ML) in the DOF corresponding to translation where the four wires are connected. The second BC restricted the deformation of the wires axially and this was because the deformation of the wires was unessential to the analysis. The only load that was applied on the structure was the gravity. The gravity was linearly increased for each step in the simulation. In the first step the gravity was increased to $0.1 g$, the second is unchanged, the third up to $1 g$ and in the fourth and final step increased up to $30 g$. The BCs and the load applied on each step are shown in Tab. 4.2.

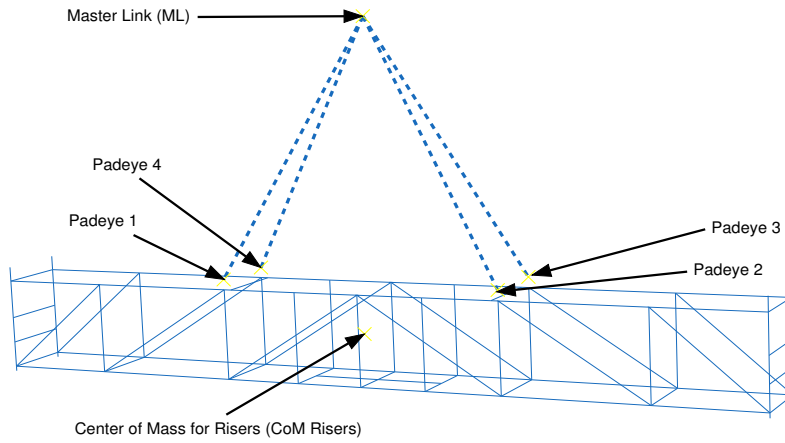
Table 4.2: Step configuration.

Step No.	Step name	Step Description	At Padeye center	At ML	Slings BC
0	Initial	Initiate B.C	U1=0 U2=0 U3=0	U1=0 U2=0 U3=0	-
1	Apply Gravity	Apply 0 – $0.1g$	U1=0 U2=0 U3=0	Propagated	-
2	Dummy	Propagated	Unlocked	Propagated	Axial dir. U1=0
3	Apply Gravity	Apply $0.1 - 1g$	Propagated	Propagated	Propagated
4	Apply Gravity	Apply $1 - 30g$	Propagated	Propagated	Propagated

The configurations from step number 0 and up to 2, stabilizes the simulation while step number 3 and 4 will gradually increase the gravity load. This loading procedure is very common in the offshore industry and is recommended according to internal best practice provided from Aker Solutions.



(a)



(b)

Figure 4.14: Position of the master link (ML), padeyes and center of mass for the risers (COM) for the calculation models.

4.1.5 Mesh

In this section the mesh types will be presented for the two calculation models. The shell and beam models were meshed with simply linear elements. Quadratic elements were used for both calculation models in order to verify the models. Only the finest mesh size of 16 mm was simulated with quadratic elements.

Table 4.3: Mesh information for the shell calculation model made of linear elements.

Global seed size [mm]	Total no. of elements	Total no. of nodes	S4R	S3	C3D8R
50	22709	22042	22327	382	3600
30	63582	65024	59336	646	3600
20	140649	141719	136405	644	3600
16	216094	216644	211320	1174	3600

Table 4.4: Mesh information for the shell calculation model made of quadratic elements.

Global seed size [mm]	Total no. of elements	Total no. of nodes	S8R	STR165	C3D8R
16	216094	639662	211320	1174	3600

Tab. 4.3 illustrates the mesh sizes for the shell model. S4R, S3 and C3D8R are the different elements in the model. The element type S4R is a linear quadrilateral element, S3 is a linear triangular element and C3D8R is a linear hexahedral element. These elements is explained in more detail in the Chapter 2. The quadratic elements, S8R, STR165 and C3D8R are used in the shell model, see Tab. 4.4

Table 4.5: Mesh information for the beam calculation model.

Global seed size [mm]	Total no. of elements	Total no. of nodes B31/B32	B31	B32
50	2528	2479/-	2528	-
30	4206	4157/-	4206	-
20	6300	6251/-	6300	-
16	7896	7847/15743	7896	7896

The beam model was meshed similarly as the shell model with the same global seed sizes as can be seen in Tab. 4.5. B31 is the linear beam elements while B32 is the quadratic element. The quadratic element was only used with the finest mesh size, 16 mm.

4.2 Convergence Analysis

A mesh convergence will be performed in order to obtain an accurate size of element for the analysis. The finite element size is of importance and has a big impact on the results obtained from the simulations. Therefore a mesh convergence will be implemented in the beginning of the FE-analysis. Mesh convergence study usually contains an increase of elements while the mathematical model is converging to an unique solution. Hence, in linear elastic analysis there exist an unique exact solution to the mathematical model. [2]

4.3 Placement of the Local Coordinate System

In order to measure the deformation on an arbitrary location in the model without including the rigid body motion a local coordinate system has to be located into the model. The location for the local coordinate system must be the same in both the shell and the beam model in order to make the appropriate comparison. The initial deformation gradient which is when the material is deforming elastically will differ depending on where the local coordinate system is placed. Therefore the chosen location was placed at the same position for both models, shown in Fig. 4.15.

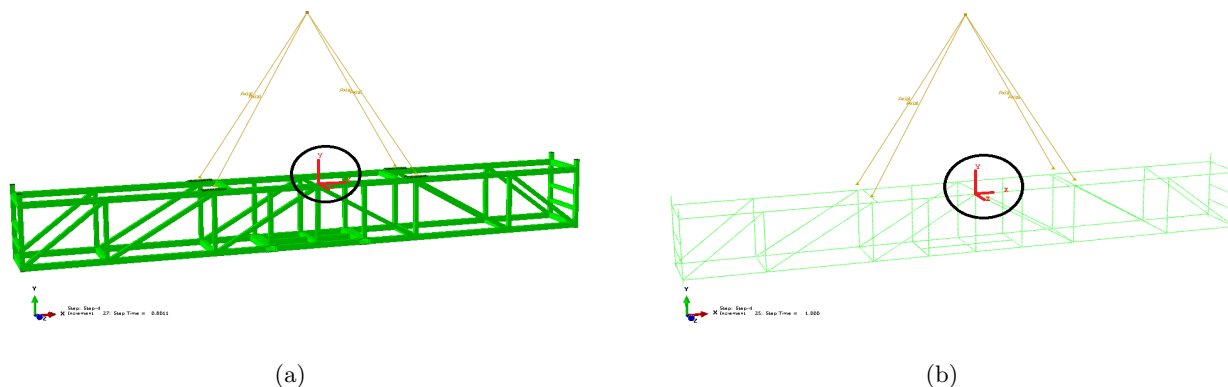


Figure 4.15: Placement of the local coordinate system in order to prevent rigid body motion effects.

4.4 Critical Area

The measurement of the deformation will be made at a critical location, as in this case at the outer support in which the largest mass proportion was applied. In Fig. 4.16 the von Mises stresses can be seen and it clearly shows that the critical area in this model is at the outer support due to the unsymmetric riser weight distribution.

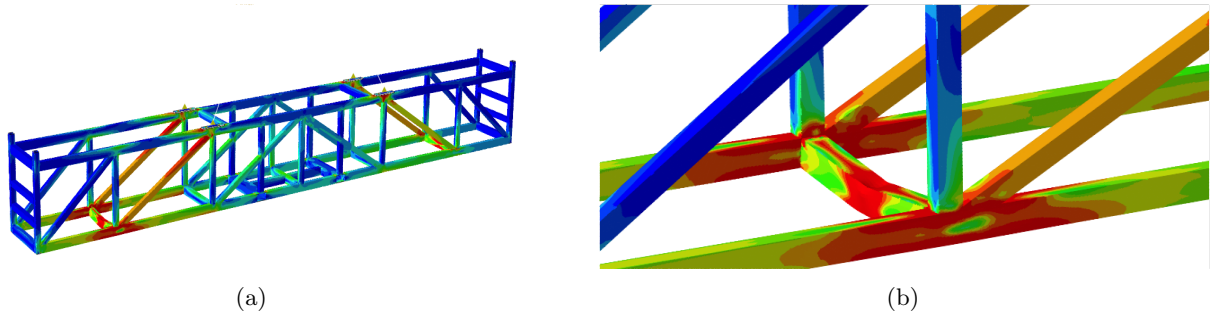


Figure 4.16: *Plot of von Mises stresses and the critical area where the deformation will be measured.*

5 Results and Discussion

In this chapter all the results from the simulations will be presented and discussed. First the mesh convergence study will be presented in order to verify the models. The result for applying the payload differently due to the risers will then be demonstrated. The capacity analysis with different mesh sizes will also be presented in order to see where collapse occurs. The influence of first and second order elements will be presented when meshing the two models with the finest mesh size of 16 mm. The results when applying different thickness integration points in the shell model will be denoted in order to verify how many points are sufficient. Lastly a comparison in capacity between the shell and the beam model will be confronted.

5.1 Mesh Convergence

Mesh convergence study consisted of measuring the von Mises stress at the bottom side of the basket along the path on the critical support, see Fig. 5.1 and Fig. 5.2.

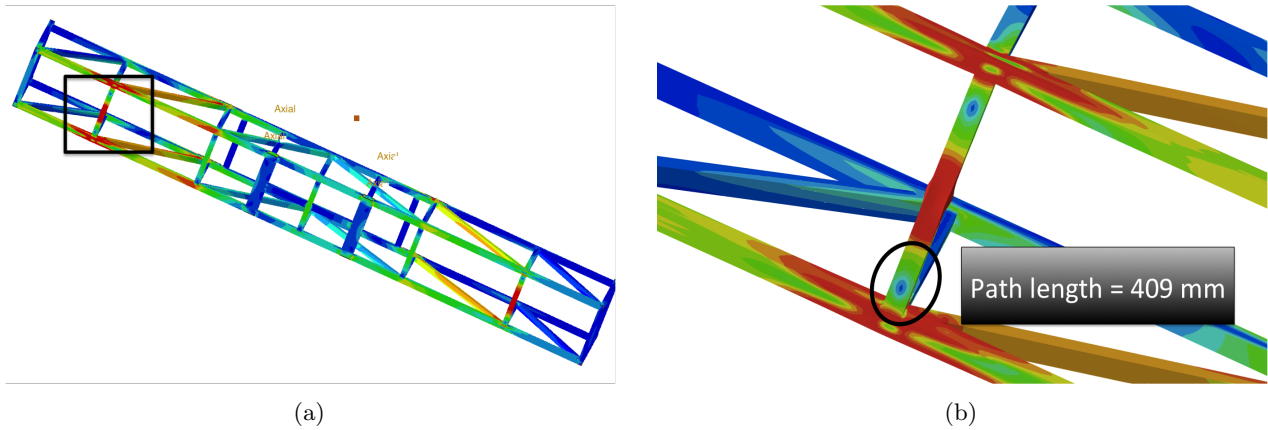


Figure 5.1: *Bottom side of the beam model where the von Mises stress was measured.*

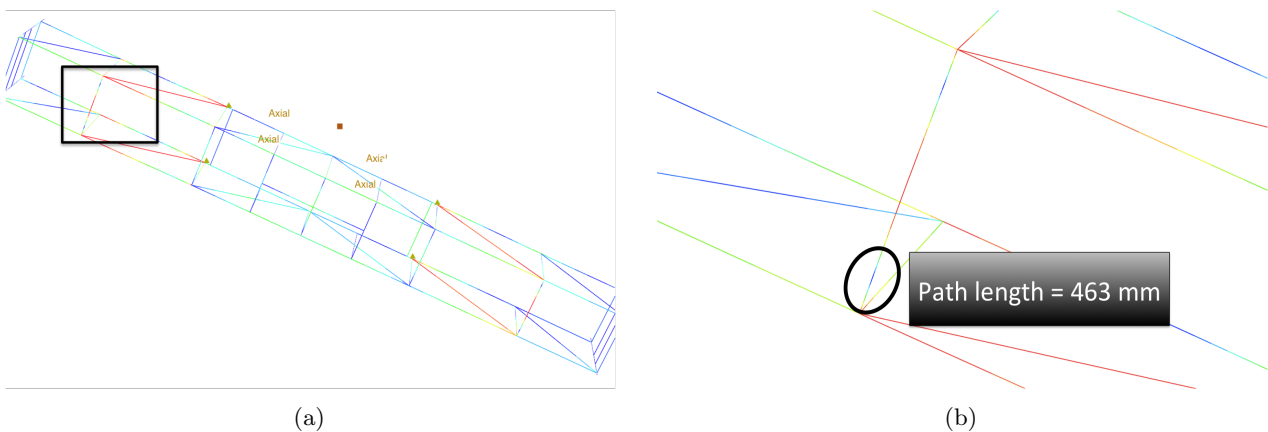
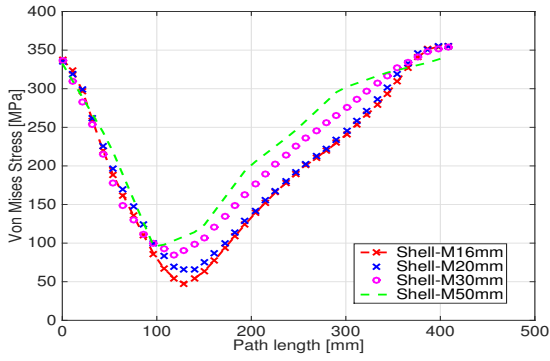
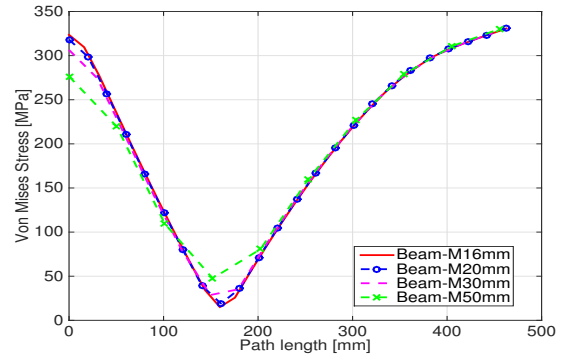


Figure 5.2: *Bottom side of the shell model where the von Mises stress was measured.*

The von Mises stress along the path for the two models are seen in Fig. 5.3 (a) and (b). It can be seen that the valley increases and converges with a finer mesh size. The curve has almost converged to the same valley in the beam calculation model with a mesh size of 16 mm (Fig. 5.3 (b)). The shell calculation model is still converging and demands a finer mesh size than 16 mm.



(a) Mesh convergence for the shell calculation model.



(b) Mesh convergence for the beam calculation model.

Figure 5.3: von Mises stress along the path length indicated in Fig. 5.1 (b) and Fig. 5.2 (b)

The results can be seen in Tab. 5.1 and Tab. 5.2. If the change in mean von Mises stress along the path was less than 1 % it was considered to be fully converged. The change between 20 mm and 16 mm for the shell model is 2.8 % and not fully converged according to the convergence criteria, but since the model was computational demanding it was interesting to check when collapse occurs for the different mesh sizes in order to see if the mesh size has an impact to it. The capacity analysis for the different mesh sizes will be demonstrated in Section 5.3

Table 5.1: The mesh convergence result for the shell calculation model.

Model name	Mesh size [mm]	Mean von Mises stress [MPa]	Change [%]
Shell-M16mm	16	201.8	2.8
Shell-M20mm	20	207.6	6.0
Shell-M30mm	30	221.9	6.3
Shell-M50mm	50	236.9	–

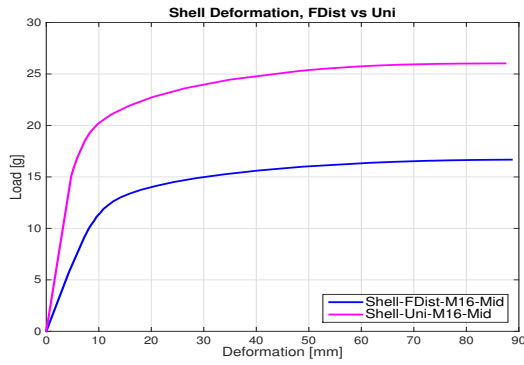
Table 5.2: The mesh convergence result for the beam calculation model.

Model name	Mesh size [mm]	Mean von Mises stress [MPa]	Change [%]
Beam-M16mm	16	199.7	0.4
Beam-M20mm	20	200.4	1.3
Beam-M30mm	30	202.3	3.0
Beam-M50mm	50	204.1	–

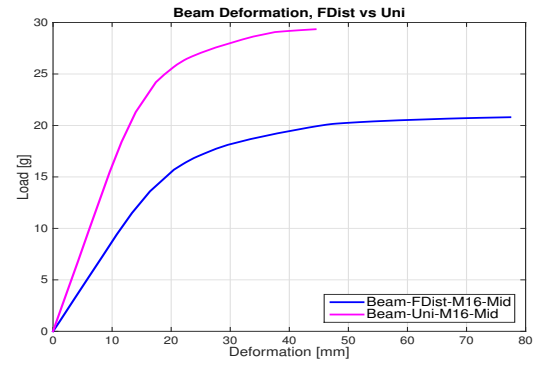
Mesh convergence study was also made with the element sizes of 14 mm, 12 mm and 10 mm for the shell model in order to see if the mean von Mises stress had fully converged at these mesh sizes. It could be seen that the change between 16 mm and 14 mm was less than 1%. This can be seen in App. E.

5.2 Distribution of Payload due to the Risers

The mass of the risers was implemented on the calculation models with two different techniques. When the mass of the risers was uniformly distributed from the COM of the risers, the collapse occurred at 16.2 g for the shell model and 18.4 g for the beam model at the critical support. But when the mass distribution was calculated analytically collapse occurred at a lower gravity multiplier which was at 10.2 g for the shell model and 13.6 g for the beam model. Both shell and the beam model are giving the same behavior. This can be seen in Fig. 5.4 (a) and (b). The reason for this is that when the mass proportion is calculated analytically and applied on each support individually the proportion of the riser mass on the critical support will be greater than the proportion would be if the riser mass would be applied uniformly from the risers COM. These differences in collapse load is pretty significant which shows that it is very important to implement the load correctly in order to make a conservative model.



(a) Shell model.



(b) Beam model.

Figure 5.4: Ultimate capacity result when the calculation models are applied with payload distribution manually and payload distribution uniformly.

The results at collapse, c are presented in Tab. 5.3 where the maximum displacement and the maximum plastic strain are measured for the calculation models.

Table 5.3: Results at collapse load.

Model	Collapse, c	Max. Disp. [mm]	Max. Plastic strain [%]
Shell Uniform	16.2	5.6	0.08
Shell Mass dist.	10.2	8.6	0.10
Beam Uniform	18.4	11.6	0.03
Beam Mass dist.	13.6	16.4	0.10

Collapse load, F_{rK} was calculated according to the acceptance criteria in Sec. 3.3 and is again defined in Eq. (5.1).

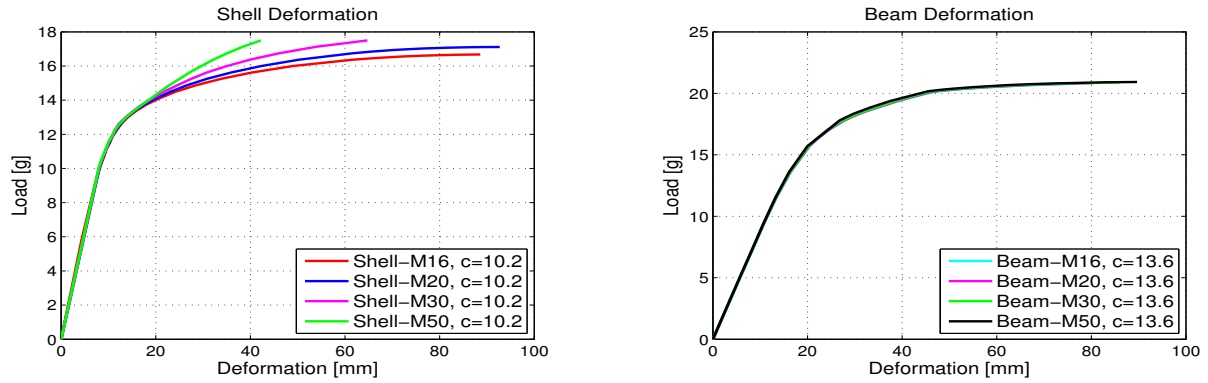
$$F_{rK} = MGW \times c \times g \quad (5.1)$$

where

$$MGW_{shell} = 16.17 \text{ tons} \quad MGW_{beam} = 16.18 \text{ tons} \quad c = \text{collapse} \quad g = 9810 \text{ mm/s}^2$$

5.3 Capacity Analysis - Collapse Load

The deformation for both shell and the beam model has been simulated with four different mesh sizes and are plotted in Fig. 5.5. The deformation is measured in the middle of the critical support shown in the previous Section 4.4, Fig. 4.16. When simulating with the four different mesh sizes, collapse has been reached before the divergence occurs in the curves. This collapse occurrence happens at 10.2 g for the shell model and 13.6 g for the beam model. This indicates the mesh size of 16 mm being converged since the collapse load is at the same place for the four different mesh sizes in both models. In the beam model there is no difference when decreasing the mesh size from 50 mm to 16 mm which means that the mesh has already converged at a mesh size of 50 mm for the beam model.



(a) Deformation on critical support for different mesh sizes for shell model, collapse (c) happens at 10.2 g (b) Deformation on critical support for different mesh sizes for beam model, collapse (c) happens at 10.2 g

Figure 5.5: Ultimate capacity result when the calculation models are applied with payload distribution manually and payload distribution uniformly.

5.4 First and Second Order Elements

In order to determine if the collapse load would have been better modeled with higher order elements, the basket was meshed with a quadratic elements for both shell and beam models with a mesh size of 16 mm. Fig. 5.6 shows that the difference is none existing between linear and quadratic elements for the beam model and do not have an impact of the load-displacement curve. This is because the mesh has already been fully converged at current mesh size. While on the other hand when the shell model is meshed with quadratic elements it does have an impact on the load-deformation curve. The difference occurs in the plastic region after collapse has been reached. The reason for this is that the mesh size is not sufficiently small when modeling the plasticity as discussed in Sec. 5.1. Quadratic elements gives a better representation of the deformation than the linear elements does and this is because the shape functions is made of second order polynomial. But in this case when collapse occurs before the two curves diverges (10.2 g), linear elements in sufficient. The reason that the quadratic element model has not been simulated past a deformation of 40 mm in Fig. 5.6b, is due to a very small step increment would have been needed and the time for the simulation would have taken to long to run.

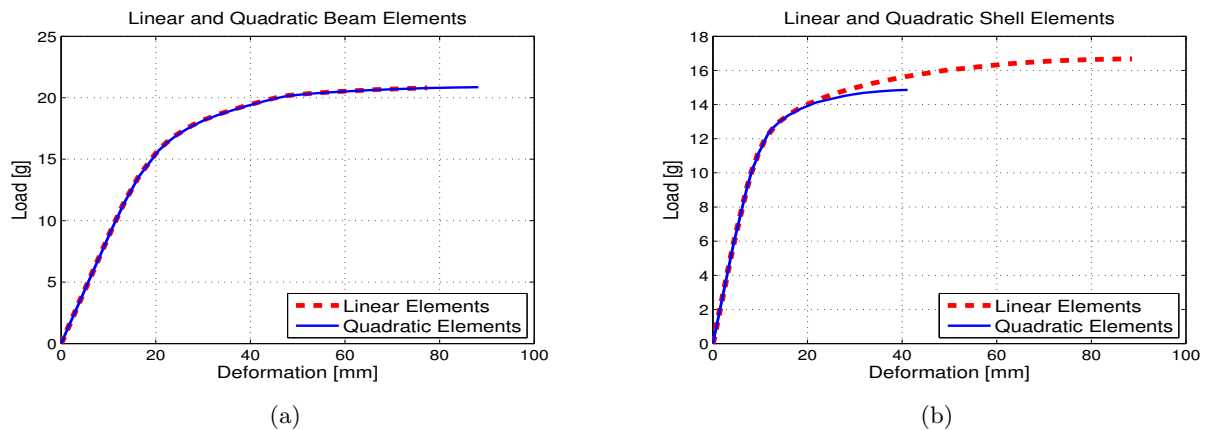


Figure 5.6: Linear compared to quadratic elements.

5.5 Thickness Integration Points

It is of interest to investigate how the number of thickness integration points affect the results for the shell model. At this time Aker Solution uses five integration points which is the default value in Abaqus. In Fig. 5.7 the deformation for the different number of integration points have been plotted. If the thickness integration points are reduced to three the deformation will at a certain point increase asymptotically earlier than higher

number of integration points. As mentioned in Sec. 2.2.2, it would be sufficient to use three integration points if the problem would be linear, but in this case the model will deform non-linear which means that three may not be sufficient. Since in this case the basket is deforming non-linearly, three thickness integration points are indeed not sufficient. There is no difference in the deformation behavior when the integration points are increased from five to seven or even as high as eleven. This means that the number of integration points of five is enough to model the plastic behavior that the material experience during the deformation stage. It can also be seen in Fig. 2.4 the error that remains for three integration points is higher than for five. It may be the case that the error from integrating with three points is just above a critical value which means that the error will propagate for each iteration and in the end have a bigger impact. Five integration points would not have this propagating error in this case.

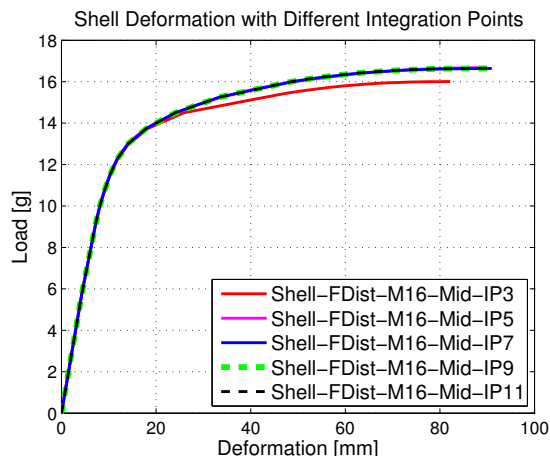


Figure 5.7: *Deformation on critical support for different thickness integration points*

5.6 Comparison between the Shell and the Beam model

As can be seen in Fig. 5.8, the model made of shell elements collapses earlier than the model made of beam elements, known since earlier to be 10.2 g and 13.6 g. In general it is known that the shell model is more flexible and gives a more accurate solution.

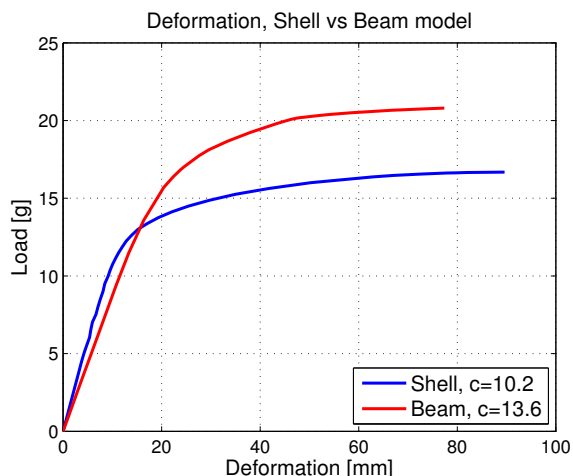


Figure 5.8: *Deformation at the critical support for shell and beam model, collapse occurs at 10.2 g for shell and 13.6 g for beam*

One reason for the lower collapse load in the shell model is the load application to the nodes. Considering the shell cross section in this case, the riser load is applied on the upper surface nodes which gives a bending moment effect, seen in Fig. 5.9 (a). The beam model is meshed with one dimensional elements and when the

riser load is applied to one node it distributes the load to the cross section. The beam's cross section remain its shape after deformation and this phenomena is shown in Fig. 5.9 (b).

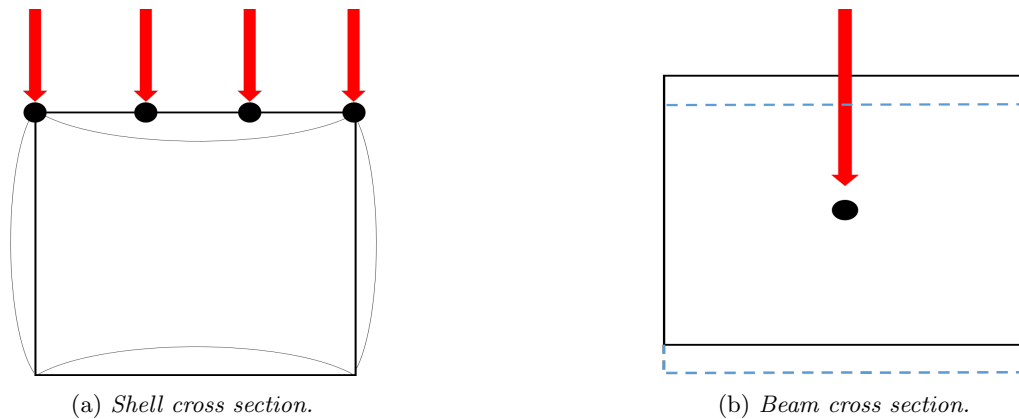


Figure 5.9: Differences in how the mass is applied to the cross section in the shell and the beam model.

In Fig. 5.8 it can also be seen that the initial deformation gradient differs between the shell and the beam model. One reason for this is the placement of the local coordinate system, it was not applied at the exact same position. The local coordinate system was placed on the corner of the cross section in the shell model and in the middle of the cross section in the beam model, see Fig. 5.10. This gives a small difference between the two models and will affect the initial deformation gradient.



(a) Placement of the local coordinate system in the shell model. (b) Placement of the local coordinate system in the beam model.

Figure 5.10: Local coordinate system placed at the top corner of the cross section in the shell model and in the middle of the cross section onto the beam model.

Another reason is that the nonstructural mass could not be applied in the exact same way to the models. The nonstructural mass was placed on the surfaces in the shell model while in the beam model it was only possible to apply it as point masses in the connections between two beam bars. This can be seen in Fig. 4.5. In order to verify the initial deformation gradient difference due to applying the nonstructural mass, it was applied in a dissimilar way in order to check the behavior, see App. F. This way of applying the mass will contribute to different mass distribution to the models and the deformation will differ from each other when applying a gradually increased gravity load.

6 Conclusions

The scope of this thesis has been to determine if it would be possible to use a beam model to simulate a normal lift case instead of using a shell model, and still be able to get a solution that is satisfying. This is something that would further the goals for the offshore industry in such a way that a lot of time could be saved for the CAE time.

When working with a geometry that is as big as the one in this thesis, a mesh size of 16 mm was enough for the beam structure but not for the shell structure when making the mesh convergence with mean Von Mises stress over the length exposed to high pressure from the risers. When measuring collapse at the critical location it was still accurate enough, see Fig. 5.5. If the mesh convergence has not fully converged to a sufficiently low tolerance another convergence test must be used later on to validate that the results from the analysis is accurate enough. In the deformation-gravity curve, collapse occurred before the different mesh sizes diverged which means that for this type of analysis the mesh had converged enough. In the beam model a mesh size of 16 mm is more than enough, and there would even be possible to use an even more course mesh size and still obtain the same result.

The results show that there is no difference in using quadratic or linear beam elements when analysing the collapse. The convergence occurred at a mesh size greater than 16 mm. The shell model, on the other hand, did not converge at the element size of 16 mm but in this case collapse had already occurred before the results diverges the quadratic elements would not be needed for this case.

It is also important to apply the payload onto the model as realistic as possible in order to obtain a more accurate solution, it could be the case that a more simple way of applying it may be more conservative but this may not always be the case. This is why it is important to investigate different options of how to apply the payload.

When there is linear deformation, only three integration points are needed when using Newton integration. If there is plastic deformation five or more integration points are needed to model a correct deformation behavior. In this case collapse load was reached before the curves diverges when checking for different number of integration points, this can be seen in Fig. 5.7. If the collapse criteria was differently defined, this may have not been the case. If there is a possibility for plastic deformation, less than five integration points will not give an appropriate solution and would not be reliable results.

The beam model experience collapse later in the gravity-displacement curve than the shell model, one reason for this is because the mass is applied on the hole cross section of the support. This means that the beam model will become more stiff when measuring deformation on the support compared to how it would have been applied in reality where it would only have contact on the top side. Another reason is because the cross section of a beam elements remain the same after deformation and can not model the bending effect in the cross section.

These limitations discussed about the beam model does not occur in the shell model, but here are a few limitations. Shell elements are not as good as beam elements when handling out of plane stresses, this means that it will become weaker when the mass from the risers are applied on the model than what would happen in reality.

No real test data has been provided from Aker Solutions so no comparison could be made between the beam model, shell model and a real case scenario. The conclusion that can be drawn is that the models have different strengths and weaknesses, and that the shell model experience collapse earlier than the beam model and therefore it is not possible to obtain the same results for the normal lift case. This makes the shell model more conservative and a better choice to utilize.

7 Future Work

The difference between a shell and a beam structure has only been analyzed for one static loading scenario with a limit analysis. It would be interesting to see if collapse would occur later if a thin solid pad would have been added to the five supports in the shell model. The results from this thesis can only be used as a source for determining if it is possible to model the structure as a beam instead of a shell model if the loading case is the same as in this thesis. It would be interesting to evaluate dynamic scenarios to see if the results will be similar to what is presented in this thesis.

References

- [1] D. AS. Standard for Certification - No.2.7-3, Portable Offshore Units (2011).
- [2] K.-J. Bathe. *Finite Element Procedures*. Prentice Hall, 1996. ISBN: 0-13-301458-4.
- [3] B. C.J and C. M.A. Numerical Integration Strategy for Plates and Shells. *International Journal for Numerical Methods in Engineering* **29** (1990).
- [4] S. Dessault. *Abaqus Online Documentation*. Version 6.14. 2014.
- [5] Durgawale. Analysis Report WP 071 Basket, Risers, riserLOCK 7.10 STRUCTURAL ANALYSIS (2014).
- [6] M. Ekh. *Mechanics of Solids - Linear Elasticity* (2013).
- [7] L. F and R. Kenneth. *Introduction to Finite Element Analysis of Plates* (2014).
- [8] D. B. J. Farnsworth. *Behavior of Shell Structures* (1999).
- [9] B. Haugen and university of Colorado. *Advanced Finite Element Methods*. 2013, pp. 1–3.
- [10] G. J Kennedy, J. S Hansen, and J. R R A Martins. *A Timoshenko Beam Theory with Pressure Corrections for Layered Orthotropic Beams* (2011).
- [11] M. Jirásek and Z. P. Bazant. *Inelastic Analysis of Structures*. Wiley, 2001. ISBN: 978-0471987161.
- [12] F. Larsson. *Non-linear Finite Element Analysis. A Short Introduction* (2010).
- [13] G. R. Liu and S. S. Quek. *The Finite Element Method: A practical Course*. Vol. 2. Elsevier Science Ltd, 2013. ISBN: 0 7506 5866 5.
- [14] O. Patrich. Calculation Report WOS ToolSkid Running,Subsea Module Vilje Sør SPS (2013).
- [15] *Review of Kirchoff Plate Theory. Kirchhoff plate theory and FE*. Michigan.gov. URL: http://www.michigan.gov/documents/mdot_RC-1441Appendix_A_102842_7.pdf.
- [16] K. Runesson. *Constitutive Modeling of Engineering Materials - Theory and Computation* (2006), 79–85.
- [17] M. Y. Shah, P. P. Timothy, and D. C. Robert. *Solid Elements with Rotational Degrees of Freedom: Part 1—Hexahedron Elements*. Vol. 31. 1991, pp. 573–592.

Appendix A Kirchhoff's Plate Theory

Kinematics

The displacement components at any point (x, y, z) in the plate are related to the in-plane displacement $\mathbf{u}^0(x, y) = [u_x^0, u_y^0]^T$ at the midplane ($z = 0$) and the transverse displacement $w(x, y)$ as

$$\mathbf{u} = \begin{bmatrix} u_x \\ u_y \end{bmatrix} = \mathbf{u}^0 - z \nabla w \quad (\text{A.1})$$

and the transverse component $u_z = w(x, y)$ is constant across the plate thickness such that $\epsilon_{zz} = 0$. From the kinematic assumption in Eq. (A.1) the in-plane strains and out-of-plane shear strains are obtained as

$$\boldsymbol{\epsilon} = \begin{bmatrix} \epsilon_{xx} \\ \epsilon_{yy} \\ \gamma_{xy} \end{bmatrix} = \tilde{\nabla} \mathbf{u} = \boldsymbol{\epsilon}^0 - z \boldsymbol{\kappa} \quad (\text{A.2})$$

$$\boldsymbol{\gamma} = \begin{bmatrix} \gamma_{xz} \\ \gamma_{yz} \end{bmatrix} = \mathbf{0} \quad (\text{A.3})$$

The auxiliary notations are introduced as

$$\boldsymbol{\epsilon}^0 = \begin{bmatrix} \epsilon_{xx}^0 \\ \epsilon_{yy}^0 \\ \gamma_{xy}^0 \end{bmatrix} = \tilde{\nabla} \mathbf{u}^0, \quad \boldsymbol{\kappa} = \begin{bmatrix} \frac{\partial^2 w}{\partial x^2} \\ \frac{\partial^2 w}{\partial y^2} \\ 2 \frac{\partial^2 w}{\partial xy} \end{bmatrix} = \nabla^* w \quad (\text{A.4})$$

with

$$\nabla^* \stackrel{\text{def}}{=} \tilde{\nabla} \nabla = \begin{bmatrix} \frac{\partial^2}{\partial x^2} \\ \frac{\partial^2}{\partial y^2} \\ 2 \frac{\partial^2}{\partial xy} \end{bmatrix} \quad (\text{A.5})$$

The strains through the thickness can not be determined from the kinematics but with the constitutive relation the out of plane strain, ϵ_{zz} can be computed when the plane stress assumption is taken into consideration.

Constitutive relations

Assuming the material to be symmetric in xy -plane and in z -direction. The stress-strain relation is then

$$\begin{bmatrix} \sigma_{xx} \\ \sigma_{yy} \\ \sigma_{zz} \\ \sigma_{xy} \\ \sigma_{xz} \\ \sigma_{yz} \end{bmatrix} = \begin{bmatrix} D_{11} & D_{12} & D_{13} & D_{14} & 0 & 0 \\ D_{12} & D_{22} & D_{23} & D_{24} & 0 & 0 \\ D_{13} & D_{23} & D_{33} & D_{34} & 0 & 0 \\ D_{14} & D_{24} & D_{34} & D_{44} & 0 & 0 \\ 0 & 0 & 0 & 0 & D_{55} & D_{56} \\ 0 & 0 & 0 & 0 & D_{56} & D_{66} \end{bmatrix} \begin{bmatrix} \epsilon_{xx} \\ \epsilon_{yy} \\ \epsilon_{zz} \\ \gamma_{xy} \\ \gamma_{xz} \\ \gamma_{yz} \end{bmatrix} \quad (\text{A.6})$$

$$\boldsymbol{\sigma} = \mathbf{D} : \boldsymbol{\epsilon} \quad (\text{A.7})$$

Noting that $\boldsymbol{\gamma} = \mathbf{0}$ in the last two rows in Eq. (A.6) since they can not determine the out-of-plane shear stress components. The plane stress condition, $\sigma_{zz} = 0$ is used to determine the relation

$$\epsilon_{zz} = -\frac{1}{D_{33}} [D_{13}\epsilon_{xx} + D_{23}\epsilon_{yy} + D_{34}\gamma_{xy}] \quad (\text{A.8})$$

By combining the Eq. (A.2) with the constitutive relation in Eq. (A.6) one obtain

$$\boldsymbol{\sigma} = \mathbf{D} [\boldsymbol{\epsilon}^0 - z \boldsymbol{\kappa}] = \mathbf{D} \boldsymbol{\epsilon}^0 - z \mathbf{D} \boldsymbol{\kappa} \quad (\text{A.9})$$

The material of the basket has an isotropic elasticity which yields the definition of the constitutive response as

$$\mathbf{D} = \frac{E}{1-\nu^2} \begin{bmatrix} 1 & \nu & 0 \\ \nu & 1 & 0 \\ 0 & 0 & \frac{1}{2}(1-\nu) \end{bmatrix} \quad (\text{A.10})$$

where E is the Young's modulus and ν is the Poisson's ratio.

The theory in this section was taken from "Introduction to Finite Element Analysis of Plates" written by Fredrik Larsson and Kenneth Runesson [7].

FE representation of Kirchhoff's plate Theory

The element stiffness matrix is calculated as

$$\mathbf{K}_e = \int_A \mathbf{B}^T \mathbf{D} \mathbf{B} dA \quad (\text{A.11})$$

where A is the domain and \mathbf{B} is the strain-displacement matrix given in Eq. (A.12) with the shape functions from the element the theory is used with. [15]

$$\mathbf{B} = - \begin{bmatrix} \frac{\partial^2 N_1}{\partial x^2} & \frac{\partial^2 N_{x1}}{\partial x^2} & \frac{\partial^2 N_{y1}}{\partial x^2} & \dots & \frac{\partial^2 N_{yn}}{\partial x^2} \\ \frac{\partial^2 N_1}{\partial y^2} & \frac{\partial^2 N_{x1}}{\partial x^2} & \frac{\partial^2 N_{y1}}{\partial y^2} & \dots & \frac{\partial^2 N_{yn}}{\partial y^2} \\ \frac{\partial^2 N_1}{\partial x \partial y} & \frac{\partial^2 N_{x1}}{\partial x \partial y} & \frac{\partial^2 N_{y1}}{\partial x \partial y} & \dots & \frac{\partial^2 N_{yn}}{\partial x \partial y} \end{bmatrix} \quad (\text{A.12})$$

The theory used here is according to Michigan's homepage [15]

Appendix B Finite Element Equations

B.1 Quadrilateral Element

Geometrical relations

The geometric relationships for a quadrilateral membrane element will in this section be presented for a warped geometry and for a flat "best fit" element, by setting the z coordinate for each node equal to zero. The non-flat relationships are used for the development of the non-linear projector for quadrilaterals while the flat projector relationships are used to develop the membrane and bending stiffness of the shell element. The following content for deriving the element stiffness matrix is taken from a course textbook made by the University of Colorado and from the textbook "The Finite Element Method: A Practical Course" written by Liu and Quek. [9],[13]

Consider a vector \mathbf{r} pointing to a non flat quadrilateral element. It can be parametrized with respect to the natural coordinates ξ and η as

$$\mathbf{r}(\xi, \eta) = \begin{Bmatrix} x \\ y \\ z \end{Bmatrix} = \begin{Bmatrix} \mathbf{N} & \mathbf{0} & \mathbf{0} \\ \mathbf{0} & \mathbf{N} & \mathbf{0} \\ \mathbf{0} & \mathbf{0} & \mathbf{N} \end{Bmatrix} \begin{Bmatrix} \mathbf{x} \\ \mathbf{y} \\ \mathbf{z} \end{Bmatrix}, \quad (\text{B.1})$$

where

$$\mathbf{x} = \begin{Bmatrix} x_1 \\ x_2 \\ x_3 \\ x_4 \end{Bmatrix}, \mathbf{y} = \begin{Bmatrix} y_1 \\ y_2 \\ y_3 \\ y_4 \end{Bmatrix}, \mathbf{z} = \begin{Bmatrix} z_1 \\ z_2 \\ z_3 \\ z_4 \end{Bmatrix}, \quad (\text{B.2})$$

where \mathbf{x} , \mathbf{y} and \mathbf{z} are the node coordinates in the global coordinate system. \mathbf{N} is the bi-linear isoparametric interpolation for the quadrilateral element

$$\mathbf{N}(\xi, \eta) = [N_1 \quad N_2 \quad N_3 \quad N_4] \quad (\text{B.3})$$

where the shape functions N_1 , N_2 , N_3 and N_4 are

$$\begin{aligned} N_1 &= \frac{1}{4}(1 - \xi)(1 - \eta) \\ N_2 &= \frac{1}{4}(1 + \xi)(1 - \eta) \\ N_3 &= \frac{1}{4}(1 + \xi)(1 + \eta) \\ N_4 &= \frac{1}{4}(1 - \xi)(1 + \eta) \end{aligned} \quad (\text{B.4})$$

The quadrilateral element can be seen in Fig. B.1 where it is transformed from the global coordinate system (x,y) to the natural coordinate system (ξ, η) .

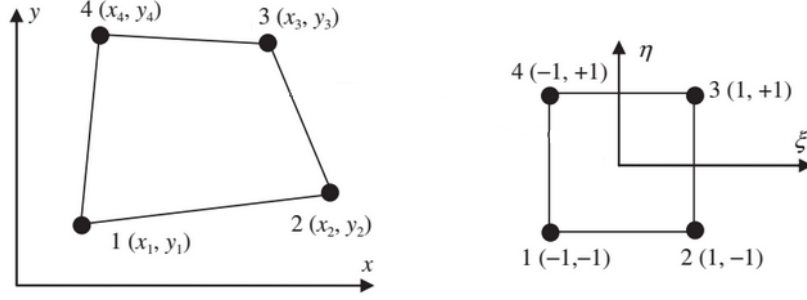


Figure B.1: *Quadrilateral element in global coordinate system (left) and natural coordinate system (right).*

The variation of the position vector \mathbf{r} can be formulated by using the geometric relations

$$\begin{Bmatrix} dx \\ dy \\ dz \end{Bmatrix} = \begin{Bmatrix} (\partial x/\partial \xi)d\xi + (\partial x/\partial \eta)d\eta \\ (\partial y/\partial \xi)d\xi + (\partial y/\partial \eta)d\eta \\ (\partial z/\partial \xi)d\xi + (\partial z/\partial \eta)d\eta \end{Bmatrix} = \begin{bmatrix} \partial x/\partial \xi & \partial x/\partial \eta \\ \partial y/\partial \xi & \partial y/\partial \eta \\ \partial z/\partial \xi & \partial z/\partial \eta \end{bmatrix} \begin{Bmatrix} d\xi \\ d\eta \end{Bmatrix} \quad (\text{B.5})$$

Eq. (B.5) can also be rewritten as

$$d\mathbf{r} = \mathbf{J}d\xi \quad (\text{B.6})$$

where \mathbf{J} is the Jacobian which is also used to compute partial derivatives with respect to the natural coordinates ξ and η . In order to obtain the *strain matrix* \mathbf{B} in Eq. (B.8), the relationship between the differentials of the shape functions with respect to x and y those with respect to ξ and η need to be formulated as in Eq. (B.7). Hence, the z coordinate is set to zero.

$$\begin{bmatrix} \partial N_i/\partial x \\ \partial N_i/\partial y \end{bmatrix} = \mathbf{J}^{-1} \begin{bmatrix} \partial N_i/\partial \xi \\ \partial N_i/\partial \eta \end{bmatrix} \quad (\text{B.7})$$

$$\mathbf{B} = \mathbf{L}\mathbf{N} = \begin{bmatrix} \partial/\partial x & 0 \\ 0 & \partial/\partial y \\ \partial/\partial y & \partial/\partial x \end{bmatrix} \mathbf{N} \quad (\text{B.8})$$

The element stiffness matrix can be obtained by using Eq. (B.9)

$$\mathbf{K}_e = \int_{V_e} \mathbf{B}^T \mathbf{c} \mathbf{B} dV = \int_{A_e} \left(\int_0^h dz \right) \mathbf{B}^T \mathbf{c} \mathbf{B} dA = \int_{A_e} h \mathbf{B}^T \mathbf{c} \mathbf{B} dA \quad (\text{B.9})$$

The integral in Eq. (B.9) can be evaluated by the following formula

$$dA = \det|\mathbf{J}|d\xi d\eta \quad (\text{B.10})$$

Then the element stiffness matrix in Eq. (B.9) can be rewritten as

$$\mathbf{K}_e = \int_{-1}^{+1} \int_{-1}^{+1} h \mathbf{B}^T \mathbf{c} \mathbf{B} \det|\mathbf{J}|d\xi d\eta \quad (\text{B.11})$$

B.2 Triangular Element

When formulating the triangular elements, the displacement \mathbf{U} is generally a function of the triangular coordinates x and y . And the displacement at any point can be expressed using the displacement at the nodes and shape functions. An arbitrary triangle and its coordinates is shown in Fig. B.2.

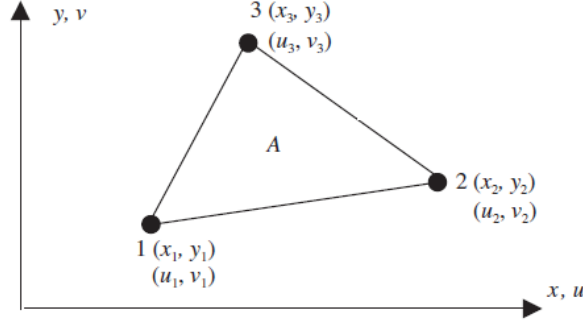


Figure B.2: *Arbitrary triangle element with coordinates.*

Then it can be assumed that

$$\mathbf{U}^h(x, y) = \mathbf{N}(x, y)\mathbf{d}_e \quad (\text{B.12})$$

where the superscript h means that the displacement is only a approximated displacement and \mathbf{d}_e is the vector of nodal displacement for the element.

$$\mathbf{d}_e = \begin{Bmatrix} u_1 \\ v_1 \\ u_2 \\ v_2 \\ u_3 \\ v_3 \end{Bmatrix} \quad (\text{B.13})$$

The shape function matrix is arranged as

$$\mathbf{N} = \begin{bmatrix} N_1 & 0 & N_2 & 0 & N_3 & 0 \\ 0 & N_1 & 0 & N_2 & 0 & N_3 \end{bmatrix} \quad (\text{B.14})$$

Eq.(B.12) is expressed in a compact matrix form, and is expressed explicitly in Eq.(B.15).

$$\begin{aligned} u^h(x, y) &= N_1(x, y)u_1 + N_2(x, y)u_2 + N_3(x, y)u_3 \\ v^h(x, y) &= N_1(x, y)v_1 + N_2(x, y)v_2 + N_3(x, y)v_3 \end{aligned} \quad (\text{B.15})$$

This means that the displacement at each point in the element is an approximation of the interpolation of the nodal displacement using the shape functions. Now the shape function N_i must be constructed for the triangular element and must satisfy the requirements: delta function property; partitions of unity; and linear field reproduction. Starting with the assumption of that the shape functions are of polynomial basis with unknown constants. Then these constants must be determined using the property of the shape functions. Normally the basic approach when constructing the shape functions $N_i (i = 1, 2, 3)$ the displacement is assumed. This works for any element type, but in this case assuming the polynomial form is more convenient. A linear triangular element are here assumed to be a linear function of x and y , and should therefore take the form as

$$\begin{aligned} N_1 &= a_1 + b_1x + c_1y \\ N_2 &= a_2 + b_2x + c_2y \\ N_3 &= a_3 + b_3x + c_3y \end{aligned} \quad (\text{B.16})$$

where $a_i, b_i, c_i (i = 1, 2, 3)$ are unknown coefficients that must be determined. There are a total of nine constants that need to be determined in Eq. (B.16). Here the property of delta function will be used, which states that

the shape function must be a unit at its home node, and zero at all the remote nodes. For this equation it will be expressed as

$$N_i(x_j, y_j) = \begin{cases} 1 & i = j \\ 0 & i \neq j \end{cases} \quad (\text{B.17})$$

When solving Eq. (B.16) with the help of Eq. (B.17) we get the constants

$$a_i = \frac{1}{2A_e}(x_j y_k - x_k y_j), \quad b_i = \frac{1}{2A_e}(y_j - y_k), \quad c_i = \frac{1}{2A_e}(x_k - x_j) \quad (\text{B.18})$$

where A_e is the area of the triangle element. Now when the shape functions have been determined the strain matrix must be derived in order to compute the stiffness matrix, in a 2D solid which a shell element basically is.

$$\epsilon_{xx} = \frac{\partial u}{\partial x}, \quad \epsilon_{yy} = \frac{\partial v}{\partial y}, \quad \gamma_{xy} = \frac{\partial u}{\partial y} + \frac{\partial v}{\partial x} \quad (\text{B.19})$$

which can be expressed in concise matrix form as

$$\boldsymbol{\epsilon} = \mathbf{L}\mathbf{U} \quad (\text{B.20})$$

Using Eq.(B.12) and Eq.(B.20), we get

$$\mathbf{B} = \mathbf{L}\mathbf{N} = \begin{bmatrix} \partial/\partial x & 0 \\ 0 & \partial/\partial y \\ \partial/\partial y & \partial/\partial x \end{bmatrix} \mathbf{N} \quad (\text{B.21})$$

Now the element stiffness matrix \mathbf{K}_e can be calculated as

$$\mathbf{K}_e = \int_{A_e} \mathbf{B}^T \mathbf{c} \mathbf{B} dV = \int_{A_e} \left(\int_0^h dz \right) \mathbf{B}^T \mathbf{c} \mathbf{B} dA = \int_{A_e} h \mathbf{B}^T \mathbf{c} \mathbf{B} dA \quad (\text{B.22})$$

Where \mathbf{c} is a material constant matrix for plane stress or plane strain and h is the thickness of the shell element. This theory used is from "The Finite Element Method: A practical Course" from Liu, G R. and Quek [13].

B.3 Beam Element

Beam element is a simple element that may be used for simple geometries. In this thesis a combination of truss elements and beam elements are used, which it called frame elements. Here the \mathbf{K}_e for a simple beam element with four DOFs will be derived, see Fig. B.3. It is usually modeled as a slender straight bar with an arbitrary cross section. It can only deform in the direction that is perpendicular to its own axis.

Fig. B.3 is illustrating a beam element with its four DOF, length and natural coordinates. The natural coordinate system is dimensionless and has its origin in the middle of the element, it has the coordinate -1 on the left side and 1 on the right side in the figure. The relation between the natural- and the local coordinate system is given in Eq. (B.23).

$$\xi = \frac{x}{a} \quad (\text{B.23})$$

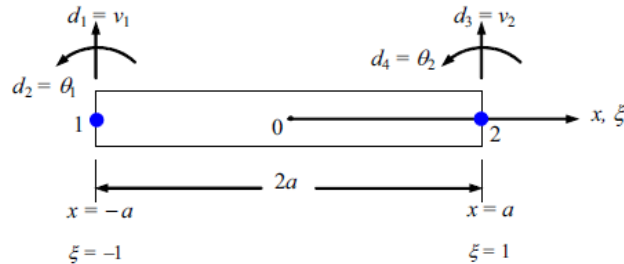


Figure B.3: *Beam element with natural coordinate system (ξ) and degrees of freedom.*

In order to derive the four shape functions in the natural coordinate system, a third order polynomial equation for the displacement is chosen Eq. (B.24) and expressed in ξ which will generate four unknown constants.

$$v(\xi) = \alpha_0 + \alpha_1\xi + \alpha_2\xi^2 + \alpha_3\xi^3 \quad (\text{B.24})$$

in vector form

$$\mathbf{v}(\xi) = \underbrace{[1 \quad \xi \quad \xi^2 \quad \xi^3]}_{\mathbf{p}^T(\xi)} \underbrace{\begin{Bmatrix} \alpha_0 \\ \alpha_1 \\ \alpha_2 \\ \alpha_3 \end{Bmatrix}}_{\boldsymbol{\alpha}} \quad (\text{B.25})$$

or

$$v(\xi) = \mathbf{p}^T(\xi)\boldsymbol{\alpha} \quad (\text{B.26})$$

In order to obtain the rotation θ , the proposed equation Eq.(B.24) must be differentiated and the relation between x and ξ must also be taken into consideration (Eq. (B.23)). This can be accomplished using the chain rule

$$\theta = \frac{\partial v}{\partial x} = \frac{\partial v}{\partial \xi} \frac{\partial \xi}{\partial x} = \frac{1}{a} \frac{\partial v}{\partial \xi} = \frac{1}{a}(\alpha_1 + 2\alpha_2\xi + 3\alpha_3\xi^2) \quad (\text{B.27})$$

In order to determine the four unknown constants in Eq. (B.24), we can use the four following conditions: at $x=-a$ or $\xi=-1$ and at $x=a$ or $\xi = -1$

$$\begin{aligned} (1) \quad & v(-1) = v_1 \\ (2) \quad & \left. \frac{dv}{dx} \right|_{\xi=-1} = \theta_1 \\ (3) \quad & v(1) = v_2 \\ (4) \quad & \left. \frac{dv}{dx} \right|_{\xi=1} = \theta_2 \end{aligned} \quad (\text{B.28})$$

When combining the conditions from Eq. (B.28) with Eq. (B.25) and Eq. (B.27), we get

$$\underbrace{\begin{Bmatrix} v_1 \\ \theta_1 \\ v_2 \\ \theta_2 \end{Bmatrix}}_{\mathbf{d}_e} = \underbrace{\begin{bmatrix} 1 & -1 & 1 & -1 \\ 0 & 1/a & -2/a & 3/a \\ 1 & 1 & 1 & 1 \\ 0 & 1/a & 3/a & 3/a \end{bmatrix}}_{\mathbf{P}} \underbrace{\begin{Bmatrix} \alpha_0 \\ \alpha_1 \\ \alpha_2 \\ \alpha_3 \end{Bmatrix}}_{\boldsymbol{\alpha}} \quad (\text{B.29})$$

Since the determinant of \mathbf{P} in Eq. (B.29) is $\neq 0$. We get

$$\boldsymbol{\alpha} = \mathbf{P}^{-1}\mathbf{d}_e \quad (\text{B.30})$$

Using Eq. (B.30) in Eq. (B.26) we get

$$\mathbf{v} = \mathbf{N}(\xi)\mathbf{d}_e \quad (\text{B.31})$$

Combining Eq. (B.26), Eq. (B.30) and Eq. (B.32) we get the \mathbf{N} vector containing the shape functions

$$\mathbf{N}(\xi) = \mathbf{p}^T(\xi)\mathbf{P}^{-1} = \underbrace{[1 \quad \xi \quad \xi^2 \quad \xi^3]}_{\mathbf{p}^T(\xi)} \underbrace{\begin{bmatrix} 2 & a & 2 & -a \\ -3 & -a & 3 & -a \\ 0 & -a & 0 & a \\ 1 & a & -1 & a \end{bmatrix}}_{\mathbf{P}^{-1}} \frac{1}{4} = [N_1(\xi) \quad N_2(\xi) \quad N_3(\xi) \quad N_4(\xi)] \quad (\text{B.32})$$

Now the shape functions are established as

$$\begin{aligned} N_1(\xi) &= \frac{1}{4}(2 - 3\xi + \xi^3) \\ N_2(\xi) &= \frac{a}{4}(1 - \xi + \xi^2 + \xi^3) \\ N_3(\xi) &= \frac{1}{4}(2 + 3\xi + \xi^3) \\ N_4(\xi) &= \frac{a}{4}(-1 - \xi + \xi^2 + \xi^3) \end{aligned} \quad (\text{B.33})$$

Now when the shape functions is established the element stiffness matrix (\mathbf{k}_e) can be derived. We start with the relation between the strain and deflection, which gives the normal stress

$$\epsilon_{xx} = \mathbf{B}\mathbf{d}_e \quad (\text{B.34})$$

where the strain matrix \mathbf{B} can be expressed with the help from Eq. (B.23) as

$$\mathbf{B} = -y \frac{\partial^2}{\partial x^2} \mathbf{N} = -\frac{y}{a^2} \frac{\partial^2}{\partial \xi^2} \mathbf{N} = -\frac{y}{a^2} \mathbf{N}'' \quad (\text{B.35})$$

The second derivative can be expressed in vector form as

$$\mathbf{N}'' = [N_1'' \quad N_2'' \quad N_3'' \quad N_4''] \quad (\text{B.36})$$

The basic formulation for the element stiffness matrix \mathbf{k}_e is then

$$\begin{aligned} \mathbf{k}_e &= \int_V \mathbf{B}^T \mathbf{c} \mathbf{B} dV = E \underbrace{\int_A y^2 dA}_{I_z} \int_{-a}^a \left\{ \frac{\partial^2}{\partial x^2} \mathbf{N} \right\}^T \left\{ \frac{\partial^2}{\partial x^2} \mathbf{N} \right\} dx = \\ &EI_z \int_{-1}^1 \frac{1}{a^4} \left[\frac{\partial^2}{\partial \xi^2} \mathbf{N} \right]^T \left[\frac{\partial^2}{\partial \xi^2} \mathbf{N} \right] a d\xi = \frac{EI_z}{a^3} \int_{-1}^1 \mathbf{N}''^T \mathbf{N}'' d\xi \end{aligned} \quad (\text{B.37})$$

This theory used is from "The Finite Element Method: A practical Course" from Liu, G R. and Quek [13].

Appendix C Material Properties

EN 10025 S355 (J0/J2) | (16mm)
=====

Material model created using:

plug-in: SAP 10001090938, ver.01

library: SAP 10001111314, ver.01

MATERIAL

name: EN 10025 S355 (J0/J2) | (16mm)

date: 26.05.2014

SAP: 10000553649

SMYS/SMTS: 355/470

thickness: t <=16

MATERIAL MODEL

temp. derating: NONE

analysis type: LIMIT

DATA SOURCES

density: ASME II, Table PRD, Carbon steels

elasticity modulus: ASME II, Table TM, Carbon Steels < 0.3%

Poisson's ratio: ASME II, Table PRD, Carbon steels

yield and tensile strengths: SAP

thermal expansion: ASME II, Table TE, Group 1

thermal conductivity: ASME II, Table TCD, Group A

heat capacity: ASME II, Table TCD, Group A

T = 20°C

E = 202350MPa

true strain	plastic strain	stress [MPa]
0.0000	0.0000	0.0
0.0012	0.0000	232.9
0.0013	0.0000	263.6
0.0015	0.0001	294.3
0.0021	0.0005	325.0
0.0039	0.0021	355.7

Appendix D Go Beam

D.1 Input data for the shell model

Version 2014.3 Date: _____

Modulus of elasticity, E
 Beam: 210000 MPa
 Columns: 210000 MPa

Beam end restraints
 Left End: Free
 Right: Free

Sway frame:

Span No	1	2	3	4	5	6
Length, m	2,19	2	2	2	2	1,81
Moment of Inertia, mm ⁴	2E+08	2E+08	2E+08	2E+08	2E+08	2E+08

Support No	1	2	3	4	5	6	7
Support coordinate, m	0	2,19	4,19	6,19	8,19	10,19	12
Vertical spring constant, N/m		1E+08	2E+08	2E+08	2E+08	1E+08	
Support type or hinge		Roller	Roller	Roller	Roller	Roller	
<i>Column under</i> Length, m							
<i>Column under</i> Moment of Inertia, mm ⁴							
<i>Column above</i> Length, m							
<i>Column above</i> Moment of Inertia, mm ⁴							
Induced support displacements, m							

Positive loads: Load case: DL

Comment	Load Type	WA N or N/m	WB N/m	LA m	LB m
	Linear	-8992,8	-8993	0	12

D.2 Input data for the beam model

GoBeam Version 2014.3 Subject: MY BEAM Checker: _____ Page: _____
 Date: _____

Modulus of elasticity, E
 Beam: 210000 MPa
 Columns: 210000 MPa

Beam end restraints
 Left End: Free
 Right: Free

Sway frame:

Span No	1	2	3	4	5	6
Length, m	2,19	2	2	2	2	1,81
Moment of Inertia, mm ⁴	2E+08	2E+08	2E+08	2E+08	2E+08	2E+08

Support No	1	2	3	4	5	6	7
Support coordinate, m	0	2,19	4,19	6,19	8,19	10,19	12
Vertical spring constant, N/m		4E+07	1E+08	9E+07	1E+08	4E+07	
Support type or hinge		Roller	Roller	Roller	Roller	Roller	
<i>Column under</i> Length, m							
<i>Column under</i> Moment of Inertia, mm ⁴							
<i>Column above</i> Length, m							
<i>Column above</i> Moment of Inertia, mm ⁴							
Induced support displacements, m							

Positive loads: Load case: DL

Comment	Load Type	WA N or N/m	WB N/m	LA m	LB m
	Linear	-8992,8	-8993	0	12

Appendix E Mesh Convergence

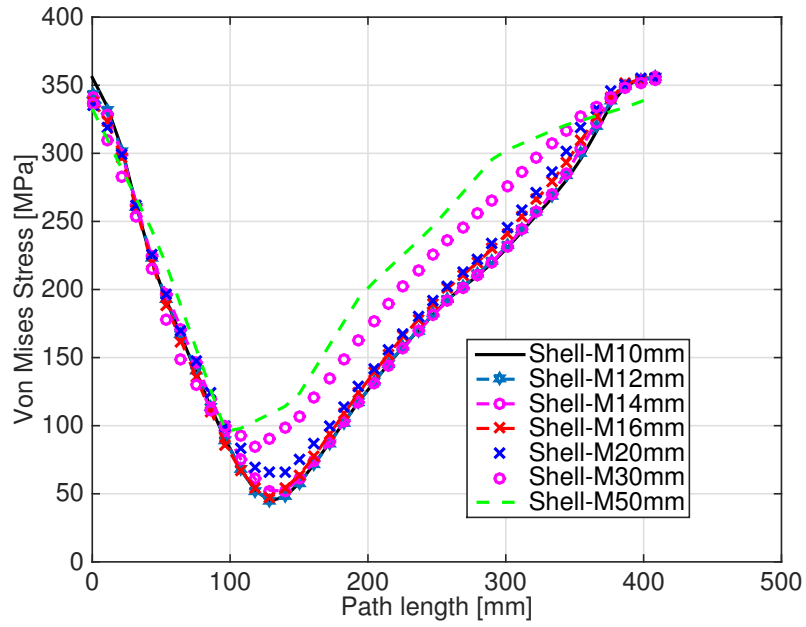


Figure E.1: Mesh convergence study with element sizes smaller than 16 mm.

Appendix F Effect of Nonstructural Mass

When applying the nonstructural mass as in Fig. F.1, the initial deformation gradient was affected as can be seen in Fig. F.2.

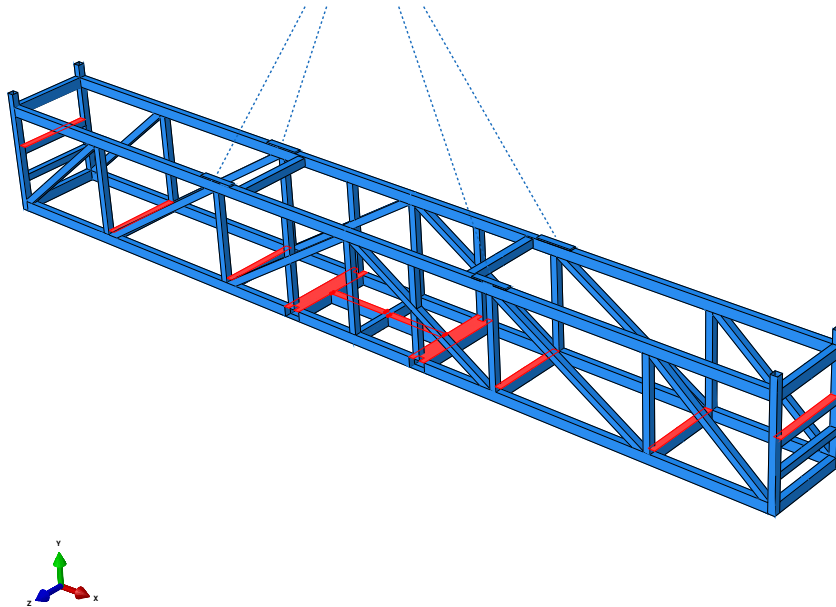


Figure F.1: *Nonstructural mass applied differently*

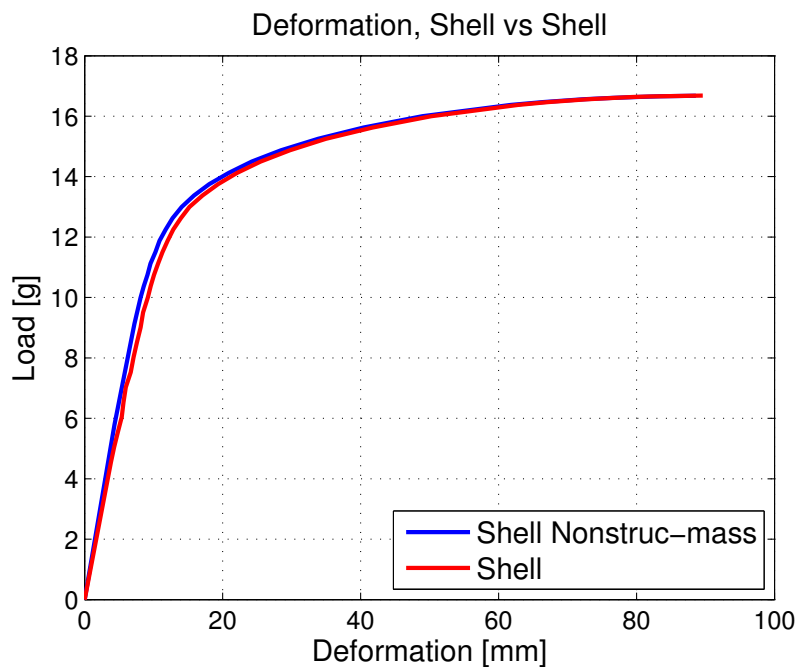


Figure F.2: *Comparison of nonstructural masses when distributing them differently*